HORIZON 2020 RESEARCH AND INNOVATION FRAMEWORK PROGRAMME OF THE EUROPEAN ATOMIC ENERGY COMMUNITY

Nuclear Fission and Radiation Protection 2018 (NFRP-2018-4)

Project acronym:	**SANDA**
Project full title:	**Solving Challenges in Nuclear Data for the Safety of European Nuclear facilities**
Grant Agreement no.:	**H2020 Grant Agreement number: 847552**

Workpackage N°:	***WP4***
Identification N°:	***D4.3***
Type of document:	***Deliverable***
Title:	REPORT ON THE EVALUATION FOR FISSION YIELDS
Dissemination Level:	***PU***
Reference:	
Status:	***VERSION 1***
Comments:	….

	Name	Partner	Date	Signature
Prepared by:	O. Serot			SEROT Olivier 169560 Signature numérique de SEROT Olivier 169560 Date : 2023.08.25 12:28:26 +02'00'
WP leader:	D. A. Rochman			Dimitri Rochman Digitally signed by Dimitri Rochman Date: 2023.08.28 10:01:01 +02'00'
IP Co-ordinator:	E. González			Signed by GONZALEZ ROMERO ENRIQUE MIGUEL - DNI ***3708** at 28/08/2023 with a certificate issued by AC Sector Público

SANDA Project D4.3: Report on the evaluation for fission yields

D. Bernard[1], A. Chebboubi[1], S. Julien-Laferriere[1], G. Kessedjian[1], O. Litaize[1], J. Nicholson[1], O. Serot[1], A. Blanc[2], H. Faust[2], U. Köster[2], P. Mutti[2], O. Méplan[3], C. Sage[3], M. Ramdhane[3], A. Letourneau[4], T. Materna[4], M. Rapala[4]

[1]CEA-Cadarache, DES, IRESNE, DER, SPRC, LEPh, F-13108 Saint Paul lez Durance (France).

[2]Institut Laue-Langevin, F-38042 Grenoble Cedex 9 (France).

[3]LPSC, Université Grenoble-Alpes, CNRS/IN2P3, F-38026 Grenoble Cedex (France).

[4]CEA-Saclay, DRF, Irfu, DPhN, LEARN, Orme des merisiers, F-91191 Gif sur Yvette (France).

Contact: olivier.serot@cea.fr Tel: +33 4 42 25 76 30.

1. Introduction

This report summarizes the work done in the frame of the 4.2.1 subtask “Evaluation of fission yields”.
Since 2007, the CEA-Cadarache, in collaboration with the Laboratoire de Physique Subatomique et Corpusculaire de Grenoble (LPSC/ CNRS), the Laue-Langevin Institute (ILL) de Grenoble and the CEA-Saclay have developed a large experience in measuring, analyzing and evaluating thermal neutron-induced fission yields. In the framework of this collaboration, a program of actinide fission yield measurements of interest for the current and innovative nuclear reactors has been initiated (see for example Ref. [Chebboubi 2021]). This program is of prime importance for many applications: estimation of the radionuclide inventories in nuclear fuel for decay heat calculation and spent fuel storage, radioprotection applications, depletion calculations in PWR cells….
Additionally, our experimental program involves a large range of observables requested to test some model assumptions implemented in the Monte-Carlo code FIFRELIN [Litaize 2015], which is a code used for fission yield evaluations.

Among these observables, two of them have been interpreted in the present 4.2.1 subtask:

- The kinetic energy dependency of the local odd-even effect for the mass A=139
- The kinetic energy dependency of isomeric ratios of ^{132}Sn.

The main aim of these works is to test both the assumption used in FIFRELIN for the sharing of the total excitation energy between both fission fragments as well as the model to generate the angular momentum of the fission fragments.

2. Kinetic energy dependency of isotopic distributions

As described in the subtask 2.5.1, the local odd-even effect for a given fission product mass was measured as a function of its kinetic energy [[Julien-Laferrière 2020a, Julien-Laferrière 2020b, Nicholson 2021]. This measurement was performed on the LOHENGRIN mass spectrometer. For a given mass A, the local odd-even effect $\delta Z(A)$ is defined as follows:

$$\delta_Z(A) = \frac{\sum_e Y(A, Z_e) - \sum_o Y(A, Z_o)}{Y(A)}$$

Where Z_e and Z_0 represent the even and odd nuclear charge, respectively.

We discuss here the case of the mass A=139 produced from the thermal neutron induced fission of ^{241}Pu. By comparing the experimental data with the prediction of the Monte Carlo code FIFRELIN [Litaize 2015], a good agreement is observed. The experimental structures can be interpreted as due to the prompt neutron emission as suggested by the contributions from the different numbers of emitted neutrons (displayed in colors on the top of Fig. 1). FIFRELIN calculations indicate that the underlying models used are well chosen in the case of a fission event involving the mass A = 139. The neutron emission probability as a function of the excitation energy shows a steplike function (see Fig. 1, bottom), which can be interpreted as the average neutron energy separation to emit 1, 2, . . . neutrons. In FIFRELIN, this process is mainly due to the temperature ratio law and the neutron transmission coefficients.

A sensitivity analysis shows that these LOHENGRIN measurements are a probe to the local prompt neutron emission through all the de-excitation path assumptions used in FIFRELIN. In particular, the temperature ratio law used in FIFRELIN to split the total excitation energy between both fission fragments seems to be pertinent.

These experimental data can be seen as a local test for the mean neutron emission and the associated neutron probabilities within a restricted preneutron mass region (here A = 139–143). Other mass regions are planned to be investigated in a similar way, in a near future and may be with other fissioning systems.

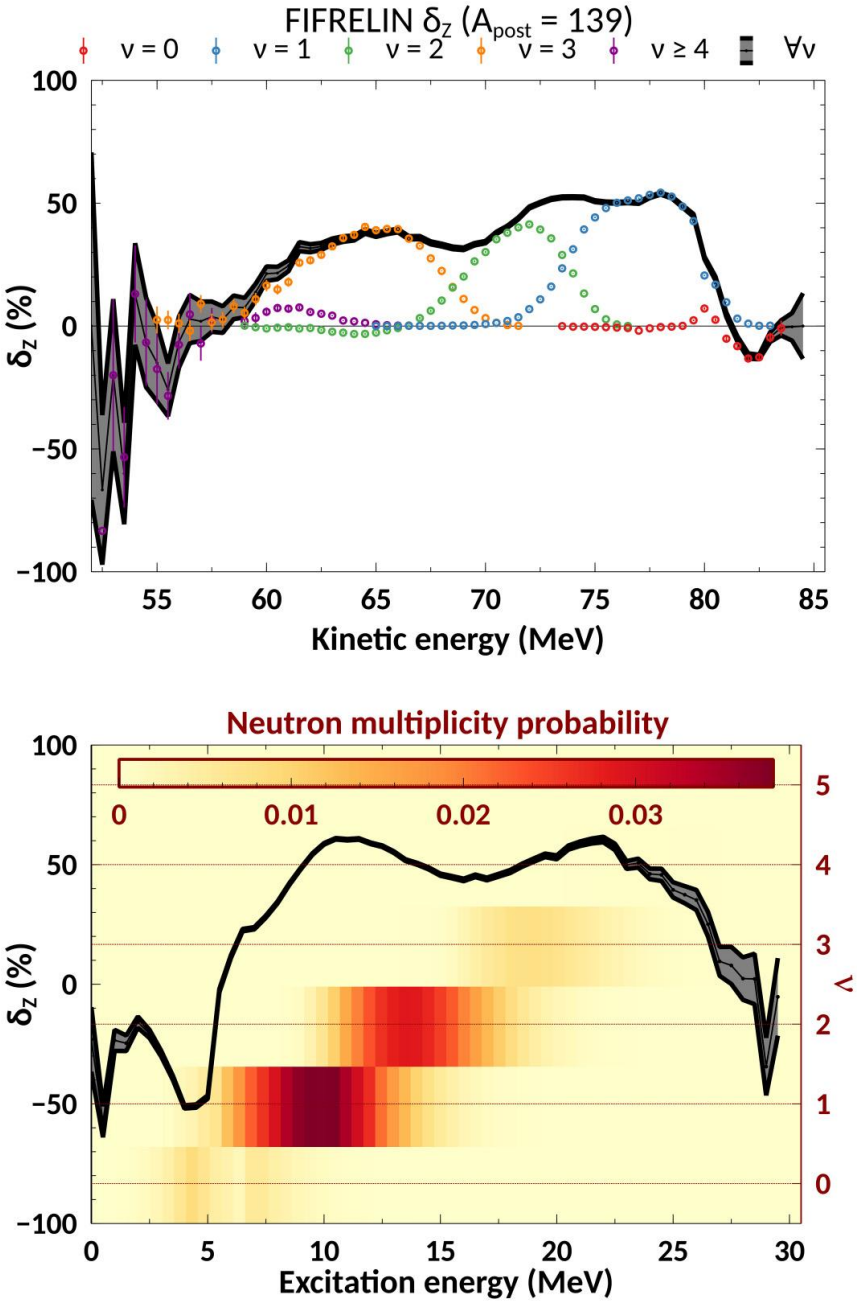

Figure 1. Top: Measured of the local odd-even effect for the mass A=139 as a function of the fission product kinetic energy (black curves). According to FIFRELIN calculations, the local odd-even structures can be explained by the several contributions from the prompt neutron emission (ν_P= 0, 1, 2, 3…in colors on the figure). Bottom: Local odd-even effect as a function of the excitation energy before neutron emission (y axis on the left). Local odd-even effect as a function of the number of emitted neutrons (y axis on the right). The associated probabilities are displayed in colors (z axis on the top). No energy loss correction is taken into account. (Figure taken from Ref. [Julien-Laferrière 2020a]).

This work was part of the article published by S. Julien-Laferrière [Julien-Laferrière 2020a].

3. Kinetic energy dependency of isomeric ratios

Another experimental campaign performed on the LOHENGRIN recoil spectrometer and described in the subtask 2.5.1 is related to the kinetic energy dependence of ^{132}Sn fission product isomeric ratio (IR) measured for thermal neutron induced fission of ^{241}Pu.
To interpret these data, we use the FIFRELIN Monte-Carlo code. Combining the measured IRs with the FIFRELIN calculations, the angular momentum distribution characterized by a free parameter J_{rms} (spin-cut-off parameter) can be deduced:

$$P(J) \propto (2J+1)\exp\left(-\frac{\left(J+\frac{1}{2}\right)^2}{J_{rms}^2}\right)$$

Figure 2 shows the evolution of the J_{rms} with kinetic energy of the doubly magic nucleus of ^{132}Sn.
It can be seen that the J_{rms} value obtained from both ^{235}U(n$_{th}$,f) and ^{241}Pu(n$_{th}$,f) [5-8] reactions are quite similar.

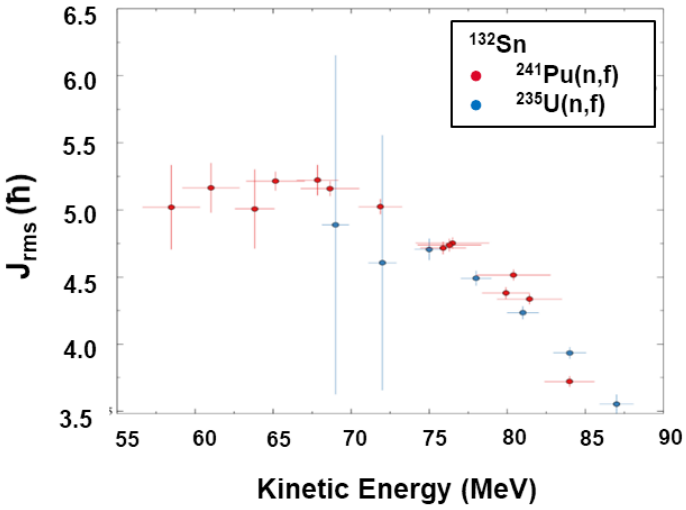

Figure 2. Average spin versus kinetic energy of the doubly magic nucleus ^{132}Sn from ^{235}U(n$_{th}$,f) [Chebboubi 2017] and ^{241}Pu(n$_{th}$,f) [N icholson 2021a, Nicholson 2021b] reactions.

In Tab. 1, our experimental isomeric ratio as well as the spin cut_off parameters deduced from FIFRELIN have been compared with the calculations from the Madland-England model [Madland 1977] (we remind that the Madland-England model is used in the JEFF-Fission-Yield library).

Experiments	<IR> (Lohengrin)	<J_{rms}> (deduced from FIFRELIN
IR of ^{132}Sn from ^{241}Pu(n$_{th}$,f)	0.0719 ± 0.0016	4.8 ± 0.1
IR of ^{132}Sn from ^{235}U(n$_{th}$,f)	0.054 ± 0.006	4.7 ± 0.2
Models		
Madland-England (a)	0.642 ± 0.039	7.5 ± 0.5
Madland-England (b)	0.0719 ± 0.0016	2.8 ± 0.1

Table 1. Average Isomeric Ratio <IR> measured on LOHENGRIN and spin cut-off parameters <J_{rms}> deduced from FIFRELIN and calculated by the Madland-Engaland model and GEF code model.

The Madland-England model uses the assumption that the isomeric ratio is only dependent on the spin of both the ground state and the isomeric state. Furthermore, it works on the supposition that all the fission fragments are characterized by a spin cut-off value of 7.5 ± 0.5 ħ which gives an isomeric ratio of 0.642 ± 0.039 for 132Sn (Madland-England (a) in Tab. 1). By using the isomeric ratio from this work, which is 0.0719 ± 0.0016, a <J_{rms}>

of 2.8 ± 0.1 (Madland-England (b) in Tab. 1) is obtained. We clearly observe a mismatch between the experimental results and those obtained from the M.E. model for 132Sn. Other experimental IR are needed in order to validate the models used in FIFRELIN for the determination of the Fission Product spin.

This work was done in the frame of the PhD thesis of J. Nicholson [Nicholson 2021a].

References

[Chebboubi 2021] A. Chebboubi *et al.*, *Measurements of U-233(n_{th}, f) fission product mass yields with the LOHENGRIN recoil mass spectrometer*. European Physical Journal A 57, (2021) 335.

[Litaize 2015] O. Litaize *et al.*, *Fission modelling with FIFRELIN*. European Physical Journal A 51, (2015) 177.

[Julien-Laferrière 2020a] S. Julien-Laferrière *et al., Investigation of neutron emission through the local odd-even effect as a function of the fission product kinetic energy.* Physical Review C 102, (2020) 034602

[Julien-Laferrière 2020b] S. Julien-Laferrière *et al., Fission fragments observables measured at the LOHENGRIN spectrometer.* European Physical Journal Web of Conferences 239, (2020) 05017

[Nicholson 2021a] J. Nicholson, PhD thesis, University Grenoble Alpes, Sept. 2021

[Chebboubi 2017] A. Chebboubi *et al.*, *Kinetic energy dependence of fission fragment isomeric ratios for spherical nuclei 132Sn*. Physical Letters B, 775, (2017) 190.

[Nicholson 2021b] J. Nicholson *et al., Investigation of fission product isomeric ratios and angular momenta of 132Sn populated in the 241Pu(nth,f) reaction*. European Physical Journal Web of Conferences 256, (2021) 00011

[Madland 1977] D. Madland and T. England, *The Influence of Isomeric States on Independent Fission Product Yields.* Nuclear science and Engineering 64, (1977) 859-865

Investigation of neutron emission through the local odd-even effect as function of the fission fragment kinetic energy

S. Julien-Laferrière,[1,2] A. Chebboubi,[1,*] G. Kessedjian,[2] O. Serot,[1] O. Litaize,[1] A. Blanc,[3] U. Köster,[3] O. Méplan,[2] M. Ramdhane,[2] and C. Sage[2]

[1] *CEA, DEN, DER, SPRC, Cadarache, Physics Studies Laboratory, F-13108 Saint-Paul-lès-Durance, France*
[2] *LPSC, Université Grenoble-Alpes, CNRS/IN2P3, F-38026 Grenoble Cedex, France*
[3] *Institut Laue-Langevin, F-38042 Grenoble Cedex 9, France*

(Dated: December 18, 2019)

Studies of new observables give different insight of the fission process. A recent experimental campaign achieved at the LOHENGRIN spectrometer aimed to extract the local odd-even effect as function of the kinetic energy, for the mass $A = 139$ in the ^{241}Pu(n_{th}, f) reaction. A comparison with the Monte Carlo code FIFRELIN permit to interpret these data in regards to the neutron emission process. The long term goal is to test if these data can validate the phenomenological temperature ratio law used in FIFRELIN to split the total excitation energy over both fission fragments.

PACS numbers: 24.75.+i, 25.85.Ec, 29.30.Aj, 23.35.+g

I. INTRODUCTION

Studies of new and current nuclear reactors rely more and more on numerical tools. Because of the growth of the computational power and the improvement of neutron transport codes, limits in precision are now shifting towards nuclear data. These data are combination of experimental and theoretical knowledge. One way to improve such data is to perform more accurate experiments and develop more physical models. In this framework, despite being discovered 80 years ago, the nuclear fission process [1, 2] persists to challenge physicists. Plenty of models are on the market with completely different fundamental hypotheses to explain this specific nuclear reaction [3–10]. Several experimental fission observables are studied such as mass and isotopic yields. Among these fission observables, an investigation of the local odd-even effect $\delta_Z(A)$ can be made.

$$\delta_Z(A) = \frac{\sum_e Y(A, Z_e) - \sum_o Y(A, Z_o)}{Y(A)} \qquad (1)$$

where indices e and o stand for even and odd respectively. The mass and isotopic yields are referred to $Y(A)$ and $Y(A, Z)$ respectively.

Moreover the dependence of $\delta_Z(A)$ on fission fragment kinetic energy could be used to deduce the sharing of the total excitation energy available at scission between both fission fragments. This determination of the excitation energy repartition is essential in the calculation of prompt neutron and gamma spectra. This observable is complementary to the isomeric ratio measurements as function of the kinetic energy [11].

In the past, the global proton odd-even effect δ_Z was investigated as function of the fission fragment kinetic energy [12–14]. It is interesting to observe that for the three reactions investigated (^{232}U(n_{th}, f), ^{233}U(n_{th}, f), ^{229}Th(n_{th}, f)), δ_Z becomes stronger at higher fission fragment kinetic energy.

In this article, we report the measurement of the local odd-even effect as function of fission fragment kinetic energy for the mass $A = 139$ in thermal neutron induced fission of ^{241}Pu.

II. EXPERIMENTAL SET-UP

The measurement of $\delta_Z(A)$ was made using the LOHENGRIN recoil separator for fission products [15] situated at the high-flux reactor of Institut Laue-Langevin (ILL) in Grenoble, France. The fission target was placed in a beam tube under a neutron flux of about 5×10^{14} n cm^{-2}s^{-1}. In order to reduce the self-sputtering of the target and improve the control of its burn-up behavior [16], the target is covered by a thin nickel foil.

The emerging ionized fission fragments will be deflected by an horizontal magnetic field followed by a vertical electrostatic field, while travelling through the spectrometer under vacuum. Fission fragments with the same mass over ionic charge $\frac{A}{q}$ and kinetic energy over ionic charge $\frac{E_k}{q}$ ratios have the same trajectory. At the end, two experimental positions are available to disentangle the triplets (A, q, E_k) selected by the LOHENGRIN spectrometer. The "straight" position is usually used to measure the mass yield by using a double anode Frisch grid ionization chamber (IC). The "curved" position take the advantage of the last focusing magnet [17] which deflects the incoming ions. This last magnet is used to increase the particle density at the focal plane position by refocusing ions with different kinetic energy. In this case, fission fragments end up on a movable tape (inside a vacuum chamber) surrounded by two clovers of four high purity germanium detectors each (HPGe). It is dedicated to the measurement of the isotopic yields through the measurement of the γ-rays characteristic for the decay of each isotope. Present results mainly come from the "curved" position setup.

III. DATA TAKING AND ANALYSIS

The local odd-even effect is directly dependent on the isotopic and mass yields. In this section, descriptions of mass and isotopic yields are shown. More details can be found in refs [18–21].

A. Mass Yield

As previously explained, the LOHENGRIN spectrometer selects triplets (A, E_k, q). To detect the mass of the incoming ions, an IC is used at the "straight" position to measure the kinetic energy and thus the associated mass. The count rate $\mathcal{N}\left(A, q, E_k \pm \frac{\Delta E_k}{2}, \Delta t_m, t\right)$ extracted from the IC is dependent on the mass A, the ionic charge q, the kinetic energy E_k, the LOHENGRIN energy resolution ΔE_k, the measurement time Δt_m, and the time since the beginning of the experiment t. Indeed since the target is under harsh conditions [16], the fissile material significantly evolves with time. To account for this effect measurement of the ionic charge distribution and kinetic energy distribution of the same mass, here $A = 136$, are regularly done across the whole experimental period. This observable is called Burn-Up (BU). Finally, the relative mass yield $\mathcal{N}(A)$ is written:

$$\mathcal{N}(A) = \sum_{E_k} \sum_{q} \frac{\mathcal{N}\left(A, q, E_k, \Delta t_m, t\right)}{BU(t) \times \Delta t_m \times E_k} \tag{2}$$

where the division by E_k account for the energy acceptance ΔE_k which is proportional to E_k. Because of the limited time, it is impossible to measure all E_k and q. Moreover, it has been shown that a correlation exists between E_k and q [18–20, 22]. In other words, the kinetic energy distribution is dependent on the ionic charges. To take into account this effect, at least three measurements of the kinetic energy distribution are done at three different ionic charges $q^{\times}_{i=1\ldots3}$ and a linear fit is performed between the mean kinetic energy $\overline{E_k}$(and the standard deviation σ_{E_k}) as a function of the ionic charge.

Therefore, three estimations of the mass yield are now achieved. These yields are then combined to have one final estimation of the mass yield $\left(\overline{\mathcal{N}}(A)\right)$ considering the correlation coming from $P(q)$ and the BU. If the three estimations are not in agreement, an additional uncertainty is calculated [20]. This additional uncertainty reflects the dispersion of the measurements. At the end, the absolute mass yield is:

$$Y(A) = 2 \times \frac{\overline{\mathcal{N}}(A)}{\sum_A \overline{\mathcal{N}}(A)} \tag{3}$$

B. Isotopic Yield

Assessment of nuclear charge of fission fragments is made through the measurement of the associated β^- delay γ emission. To detect these γ-rays, two clovers of 4 HPGe each surrounding a vacuum chamber with a movable tape are used at the "curved" position. Concretely the beam associated to a specific triplet selection (A, q, E_k) is implanted on the movable tape. During the implantation, the associated γ-rays are recorded. After typically 30 minutes, the beam and the acquisition are stopped. The tape is then moved to remove the remain radioactivity. A new measurement (still with the beam off) of 30 minutes is started in order to estimate the background coming from the vacuum chamber. Indeed the beam is not perfectly collimated. Thus, certain amount of ions are implanted on the vacuum chamber instead of the movable tape. After the background measurement, the LOHENGRIN setting is changed to a new triplet selection (A, q', E'_k) and a new collection is started. Figure 1 shows the principle of the method. For a given mass, because of the limited time, only the ionic charge distribution is measured with the γ detectors at a given kinetic energy $E^{\times}_k$. The number of decays N_d of an isotope is written:

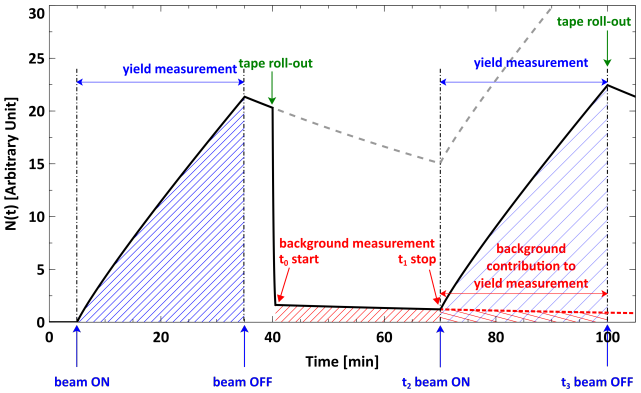

FIG. 1: (Color online)Scheme of the isotopic evolution $N(t)$ over time. The full lines correspond to the isotopes on the tape and on the vacuum chamber. When the tape is moved and the LOHENGRIN setting changed, a background coming from ions implanted into the window support grid and ions scattered to the vacuum chamber walls, can be detected and must be subtracted.

$$N_{d_\gamma}\left(Z, q|E^{\times}_k\right) = \frac{N_\gamma\left(Z, q|E^{\times}_k\right)}{\epsilon_\gamma I_\gamma f_\gamma} \tag{4}$$

The count rate N_γ is extracted using the Program Tv [23]. The efficiency ϵ_γ is extracted from a Monte Carlo simulation of the experimental setup and validated against experimental data from point sources (^{60}Co, ^{133}Ba, ^{207}Bi) and online beam isotopes (^{96}Y, ^{134}Te) covering the range 100 keV - 2.3 MeV. The intensity I_γ is coming from a nuclear database [24]. The intensity can be split into a relative factor I^{rel}_γ and normalization factor I^{γ}_{norm}: $I_\gamma = I^{\text{rel}}_\gamma I^{\gamma}_{\text{norm}}$. Finally, the sum effect correction factor $f\gamma$ is calculated with the TrueCoinc software [25]. This factor reflects the mis-

estimation of the detected γ transition. Indeed, sometimes two successive γ-rays (E_{γ_1}, E_{γ_2}) of the same cascade can be detected simultaneously as one γ transition ($E_\gamma = E_{\gamma_1} + E_{\gamma_2}$). At this step, different γ-rays are used to estimate a mean $\overline{N_d}$. As previously shown, if these different γ-rays are not in agreement, an additional uncertainty is taken into account. Also, only contributions coming from fission (and not from the deposit background) are of interest. By solving the Bateman equations, the corrected number of decay N_{d_f} is written:

$$\overline{N_{d_f}}\left(Z,q|E_k^\times\right) = \overline{N_d}\left(Z,q|E_k^\times\right) - \overline{N_{d_{bkg}}}\left(Z,q|E_k^\times\right) \quad (5)$$

However, the quantity of interest is the fission rate τ which is assessed by resolving the matrix form of the Bateman equations:

$$\boldsymbol{\tau}\left(\boldsymbol{q}|\boldsymbol{E_k^\times}\right) = \boldsymbol{B}\boldsymbol{N_d}\left(\boldsymbol{q}|\boldsymbol{E_k^\times}\right) \quad (6)$$

with $\boldsymbol{\tau}\left(\boldsymbol{q}|\boldsymbol{E_k^\times}\right)$ the vector of $\tau\left(Z,q|E_k^\times\right)$ and $\boldsymbol{N_d}\left(\boldsymbol{q}|\boldsymbol{E_k^\times}\right)$ the vector of $N_d\left(Z,q|E_k^\times\right)$. $\boldsymbol{B}$ values depend on the branching ratio (from one isotope to another), the decay probability λ of each isotope of the isobaric chain and of the acquisition time. See appendix for more details on correction involving Bateman equations.

To assess the relative isotopic yield $\mathcal{N}(A,Z)$, the fission rate must be corrected by the probability $P\left(E_k^\times\right)$ to have the fission fragment at the selected kinetic energy $E_k^\times$. However this probability depends on the ionic charge as already explained previously. This probability is then expressed as:

$$\begin{aligned} P\left(E_k^\times\right) &= \int_{E_k^\times - \frac{\Delta E_k^\times}{2}}^{E_k^\times + \frac{\Delta E_k^\times}{2}} \rho(E_k)\,\mathrm{d}E_k \\ \rho(E_k) &= \frac{1}{\sqrt{2\pi}\sigma_E(q)} \exp\left(-\frac{\left(E_k - \overline{E_k}(q)\right)^2}{2\sigma_{E_k}(q)^2}\right) \end{aligned} \quad (7)$$

The quantities $\overline{E_k}(q)$ and $\sigma_{E_k}(q)$ are derived from the measurement, with the IC, of the (at least) three different kinetic energy distributions. A linear evolution is expected for both quantities. Note that this approach implies two approximations. Firstly a Gaussian form of the kinetic energy distribution is supposed. Secondly, the probability $P(E_k)$ is supposed to not be dependant on the isotope. Indeed the kinetic energy distribution measured with the IC is related to the mass (here $A = 139$) and not the isotope. Also, the correction due to the target Burn-Up is taken into account for each ionic charge measured (at time t_q). $\mathcal{N}(Z)$ is then written:

$$\mathcal{N}(Z) = \sum_q \frac{\tau\left(Z,q|E_k^\times\right)}{BU(t_q) \times P\left(E_k^\times\right)} \quad (8)$$

The absolute normalization is achieved in two step. First the isobaric chain $A = 139$ is considered as a reference.

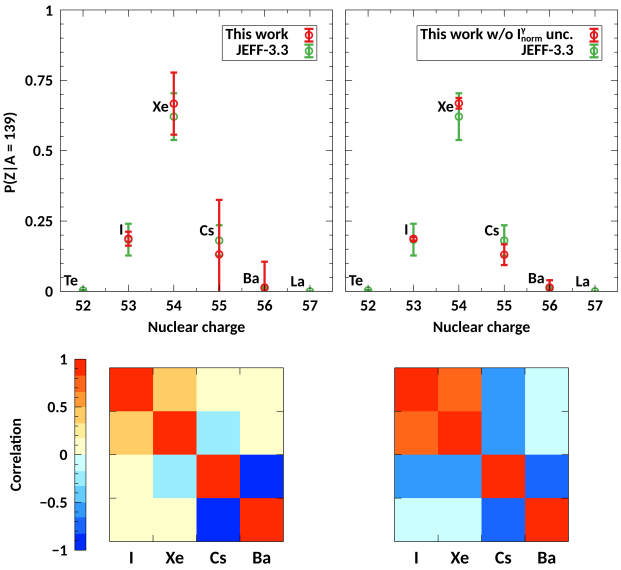

FIG. 2: (Color online)Absolute isotopic yields for the mass $A = 139$ with all the uncertainties propagated (left) and for the case where $\Delta I^\gamma_{\mathrm{norm}} = 0$ (right). Correlation matrices in both cases are also computed (bottom).

Indeed for this chain, four isotope ^{139}I, ^{139}Xe, ^{139}Cs and ^{139}Ba are detected. The cumulative yield of these 4 isotopes corresponds approximately to 99.5 % of the mass yield (which was measured with the ionization chamber setup) according to the nuclear data libraries [26, 27]. The bias from the non-observed 0.5 % is negligible in comparison to the other sources of uncertainties. Then it can be written:

$$Y(A = 139) = k_{139} \sum_Z \mathcal{N}\left(Z|A = 139\right) \quad (9)$$

Finally for all masses and isotopes, the isotopic yields can be written:

$$Y(A,Z) = k_{139} \times \mathcal{N}\left(Z|A\right) \quad (10)$$

Figure 2 shows the absolute isotopic yields for the mass $A = 139$ with the associated covariance matrix for two cases. On the left with the actual uncertainties in I_γ and on the right with, the uncertainty of the normalization intensity I^γ_{norm} put to 0. In that case, the total uncertainty is reduced by a factor of 4. The covariance matrix is also completely different. In other words, the uncertainties are mainly coming from nuclear data. By improving these data, more accurate isotopic yields can be extracted. Finally, a comparison with the JEFF-3.3 database is also displayed and shows an overall good agreement. These data were recorded in May 2013 [] using a 282 μg.cm^{-2} of ^{241}Pu on 7×0.5 cm^2 target covered by a thin nickel foil ($\approx 0.25\mu$m). This campaign was made to measure isotopic yields for 8 masses.

IV. FROM LOCAL ODD-EVEN EFFECT TO NEUTRON EMISSION USING FIFRELIN

In this work, a focus on the local odd-even effect $\delta_Z(A)$ as function of the kinetic energy for the mass $A = 139$ is done. An experimental campaign in July 2016 [] with a thinner target (208 μg.cm^{-2} of ^{241}Pu on 7×0.5 cm^2) covered by a thin nickel foil ($\approx 0.25\mu$m) was made for this specific purpose. Here all the steps to extract isotopic yields won't be made. Since an evolution as function of the kinetic energy is investigated, it is not needed to correct from $P(E_k)$. In this framework, the absolute normalization is also not necessary. To reduce the uncertainties and have a more discriminant quantity, the observables of interest are the 30 min isotopic cumulative yields N_c:

$$N_c\left(Z|A, E_k^{\times}\right) = \sum_q \frac{N_d\left(q|E_k^{\times}\right)}{BU\left(t_q\right)} \tag{11}$$

To interpret the results, a comparison with the Monte Carlo FIFRELIN is performed. The aim is to test FIFRELIN assumptions. If an agreement is reached between the data and FIFRELIN calculations, it allows to look if these data can give feedback on the main ingredient of the FIFRELIN calculation (temperature ratio law for instance). However, some corrections are needed to go from the calculations (which directly reflect the fission process) to the experimental data. First, an energy loss correction must be done, then the Bateman equation resolution would be applied B^{-1}. In the following details, on FIFRELIN are presented, such as the energy loss correction process. Then a sensitivity study on the main ingredient of the simulation will be shown.

A. FIFRELIN

FIssion Fragment Evaporation Leading to an Investigation of Nuclear data (FIFRELIN) [28–30] is a Monte Carlo code developed at CEA Cadarache since 2010. Initially, the aim is to describe the de-excitation of fission fragments from their formation (after being fully accelerated) until reaching thier ground state or a metastable state decaying through β decays. Nowadays, the code can theoretically describe the de-excitation of any nucleus starting from a given nuclear level. FIFRELIN relies on pre-neutron nuclear data as well as models to compute the most accurate de-excitation path. The code can be separated into two parts. First, the fission process creates two fission fragments with a given mass, nuclear charge, kinetic energy, excitation energy, spin and parity. In this work, no experimental data exists for the reaction ^{241}Pu(n_{th}, f). The pre-neutron isotopic yields $Y(A, Z)$ and TKE yields $Y(TKE)$ are then coming from the GEF code [31]. The code samples the light fission fragment mass and nuclear charge in the $Y(A, Z)$ distribution. The total kinetic energy is then sampled in the $Y(TKE)$ distribution. The conservation laws permit to assess the heavy fragment characteristics and the associated kinetic energy E_k. The repartition of the total excitation energy is mainly driven by a phenomenological temperature ratio law $\mathrm{R_T}(A)$ with two free parameters $\mathrm{RT_{min}}$ and $\mathrm{RT_{max}}$. By definition, with CN standing for compound nucleus, there are three anchor points in the $(A, \mathrm{R_T})$ space :

$$\mathrm{R_T}\left(A_{\mathrm{CN}}/2\right) = 1,\ \mathrm{R_T}\left(A_{\mathrm{CN}} - 78\right) = \mathrm{RT_{min}},\ \mathrm{R_T}\left(132\right) = \mathrm{RT_{max}}$$

A linear interpolation is then made between each points. Finally the spin of each fission fragments is sampled from:

$$P(J) \propto (2J+1)\exp\left(-\frac{(J+1/2)^2}{2\sigma^2}\right) \tag{12}$$

with σ^2 a free parameter for each fission fragment region (light and heavy). Those four free parameters are fixed against a target observable. Here the total average prompt neutron multiplicity $\overline{\nu} = 2.92$ [27] was the target observable and the four parameters which reproduce this value are $\mathrm{RT_{min}} = 0.5$, $\mathrm{RT_{max}} = 1.2$, $\sigma_L = 7.2$ and $\sigma_H = 8.6$.

Secondly, both fission fragments will emit prompt (n, γ, e$^-$) particles until reaching a β decaying state. To do so, FIFRELIN completes the experimental levels coming from RIPL-3 database [32, 33] by using level density (here the Composite Gilbert and Cameron Model [34]) and spin models (here the Back-Shifted Fermi Gas Model [32, 33]). Once the level scheme is complete, the probability to go from a level i to a level j by emitting either n, γ or e$^-$ is calculated within the notion of nuclear realization [30, 35]. In this framework, different level schemes (for a given isotope) can be sampled, and for each sampled level scheme, different de-excitation paths can be computed. For each emitted particle, different ingredients are used. The probabilities associated to neutron emission are calculated thanks to neutron transmission coefficients which are derived from an optical model (here the Koning-Delaroche model [36]) used through the ECIS code [37]. The ones associated to the γ emission are derived from the γ strength function (here the Enhanced Generalized LOrentzian [38] model) and experimental information. The ones associated to the e$^-$ emission are calculated with the BRICC code [39], or coming from experimental data.

FIFRELIN can compute the isotopic yields as function of the kinetic energy through an event by event analysis. However the kinetic energy sampled by FIFRELIN need to be corrected forthe energy loss of fission fragments inside the target and its cover. To take it into account, FIFRELIN kinetic energy distributions are convoluted by a Landau distribution [40] which models the energy loss of ions through a thin layer [20, 41]. Two free parameters are adjusted in order to reproduce the experimental kinetic energy. Here the energy loss is considered identical for each isotope of a given mass. Actually, since the target and cover thickness may evolve over time (self sputtering, oxidation of Ni foil, diffusion into backing [16]), the parameters are adjusted for each BU points. So the

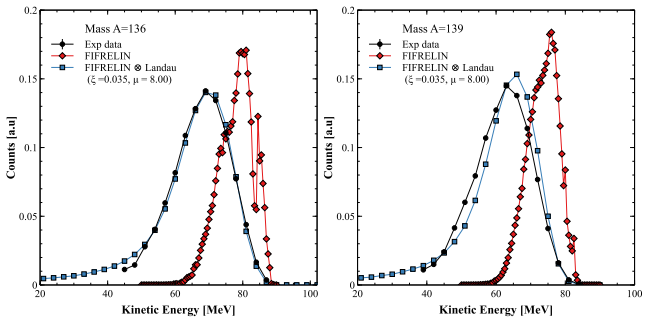

FIG. 3: (Color online)Comparison of experimental kinetic distribution (black circle) with FIFRELIN calculation(red points). An agreement is reached by convoluting FIFRELIN with Landau distribution. Parameters were fixed thanks to the mass $A = 136$ (left) and applied to mass $A = 139$ (right). The lines are to guide the eye.

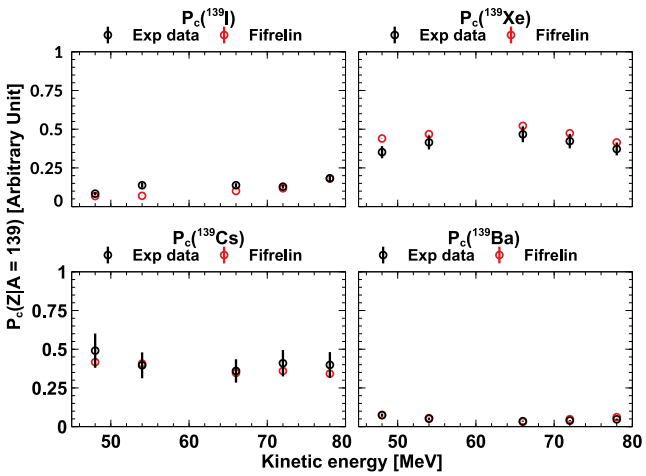

FIG. 4: (Color online)Cumulated isotopic yield probability.

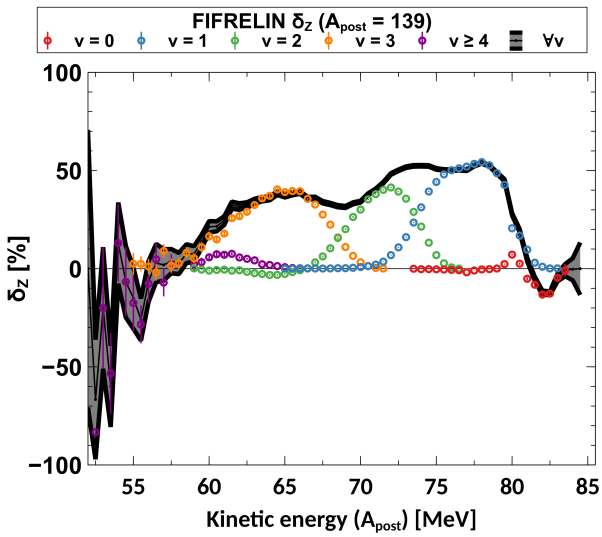

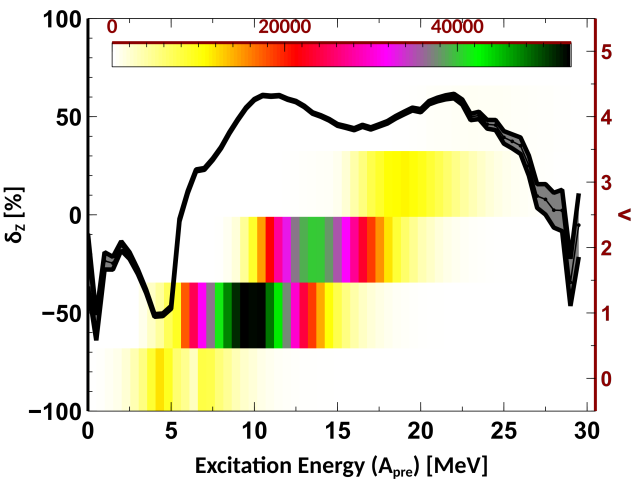

FIG. 5: (Color online)Local odd-even effect as function of the kinetic energy (top) and excitation energy (bottom). The components coming from the emission of 0, 1, 2, 3 and ≥ 4 neutrons are displayed in colors. The number of emitted neutrons (y-axis on the right) as function of the excitation energy is also shown (bottom).

mass $A = 136$ is used to fix the free parameters (see left plot of Figure 3) which are used to correct the kinetic energy distributions for $A = 139$ (see right plot of Figure 3).

The last correction of FIFRELIN data is to carry the Bateman equation solution $\boldsymbol{B^{-1}}$ on FIFRELIN instead of the experimental data to avoid additional uncertainties. Figure 4 shows the result of the comparison. The agreement between the experimental data and FIFRELIN is satisfactory. In other words, FIFRELIN is validated in regards of the kinetic energy dependence of the mass $A = 139$.

B. Test of model assumption

The next step is then to look at the local-odd even parameter as function of the kinetic energy computed by FIFRELIN without taking into account the energy loss. Figure 5 shows $\delta_Z(A)$ as function of the kinetic energy (top) and the excitation energy (bottom). The different color points represent the $\delta_Z(A)$ for fission events with different neutron emission. It seems clear that the structure of the $\delta_Z(A)$ is dependent on the emitted number of neutrons. It must be reminded that the adjusted parameters of FIFRELIN were fixed according to the average total prompt neutron emission $\overline{\nu u}$ and not using the cumulative yields of the mass $A = 139$. In this way, the predictive power of FIFRELIN can be tested with these new experimental data. Since FIFRELIN is in good agreement with these experimental data seems to imply that the underlying hypothesis used in FIFRELIN are

satisfactory. According to Fig 5, $\delta_Z(A)$ is driven by the neutron emission process. In FIFRELIN, this process is mainly due to the temperature ratio law and the neutron transmission coefficients.

A sensitivity analysis can be applied on the two main parameters of this analysis. The first one is the total excitation energy through a shift of $\pm$ 0.1 on the parameter RT_{min} (which corresponds to a shift of $\pm$ 2 MeV in excitation energy). Figure 6 shows the impact of such shift on local odd-even effect and on the cumulative isotopic yields. Relative quantities (to the reference FIFRELIN calculation) are plotted. It can be observed the temperature law modification only changes the parity at higher kinetic energy. Nevertheless the measurements are not enough accurate to provide a new constraint on this temperature law. It can be explained by the impact of the energy loss through the target. A thinner target should enhance the differences coming from initial excitation energy. These results give confidence in the models and the processes used by FIFRELIN. Finally the second sensitive parameters tested are the pre-neutron isotopic yields.

If the mean nuclear charge is shifted by $\pm$ 1 unit, simulations are no more in agreement with the experimental data as shown on Figure 7. Therefore these data can also be used to assess the pre-neutron isotopic yields as expected. At the end these data can be seen as a local test of the mean neutron emission and the associated neutron probabilities for a restricted pre-neutron mass region (here $A = 139 - 143$).

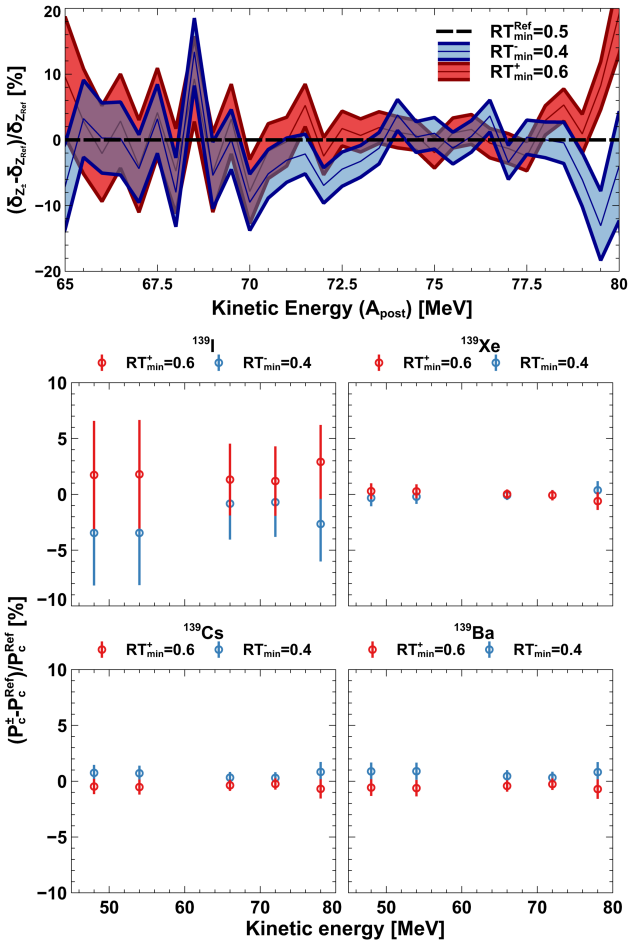

FIG. 6: (Color online)Impact of a shift of 0.1 on the parameter RT_{min}. (Top) Local odd-even effect compared with the reference FIFRELIN calculation. A slight difference can be seen at higher kinetic energy. (Bottom) Cumulated isotopic yield compared with the reference FIFRELIN calculation. No significant difference is observed.

V. CONCLUSION AND OUTLOOK

The local odd-even effect $\delta_Z(A)$ as function of fission fragment kinetic energy was assessed through measurement at the LOHENGRIN recoil spectrometer. Comparisons with the Monte Carlo code FIFRELIN were performed in order to interpret these experimental data in regards to the neutron emission process. The good match between the experimental results and the calculations coming from FIFRELIN seems to imply that the underlying models used are well chosen in the case of a fission event involving the mass $A = 139$. A sensitivity analysis shows this kind of measurements as a probe to the local pormpt neutron emission through all the de-excitation path assumptions used in FIFRELIN. However because of the energy loss inside the target, the data are not discriminant enough to highlight the impact of the initial excitation energy. These studies are complementary to the ones looking at the isomeric ratios evolution as function of fission fragment kinetic energy [11] or those looking at the correlation between the prompt γ cascade in coincidence with fission fragment and neutron observables [42–44].

VI. ACKNOWLEDGMENT

This work was supported by IN2P3, by the University of Grenoble Alpes and by “le défi NEEDS”. The authors are grateful for the support of the ILL and all the staff involved from CEA-Cadarache and LPSC.

Appendix A: Resolution of Bateman equations

In this document, we detail the way to go from the number of decays N_d of an isotope to the fission rate τ.

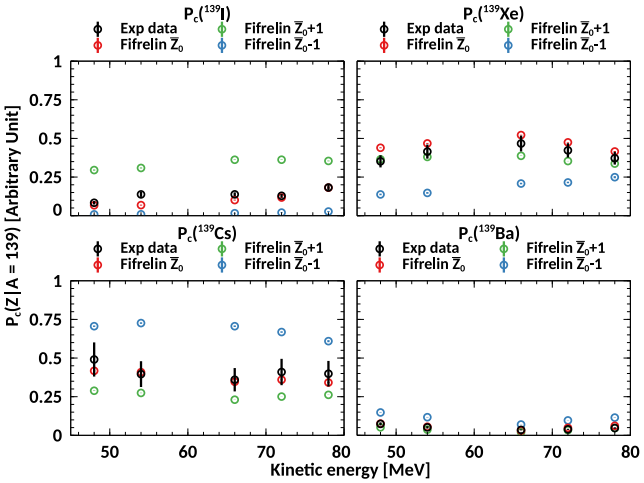

FIG. 7: (Color online)Impact of a shift of one unit of the pre-neutron mean nuclear charge for all masses. A huge impact is then observed.

With a source term τ

The activities of a decay chain are ruled by the Bateman equation:

$$\begin{aligned}\frac{dN_0(t)}{dt} &= -\lambda_0 N_0(t) + \tau_0 \\ \frac{dN_1(t)}{dt} &= -\lambda_1 N_1(t) + \tau_1 + \mathrm{BR}_{0\to1}\lambda_0 N_0(t) \\ &\vdots \\ \frac{dN_n(t)}{dt} &= -\lambda_n N_n(t) + \tau_n + \sum_{i=0}^{n-1} \mathrm{BR}_{i\to n}\lambda_i N_i(t)\end{aligned} \tag{A1}$$

with $N_{i=0,n}$ the population of the i^{th} nucleus, $\lambda_{i=0,n}$ its decay probability, $\tau_{i=0,n}$ the associated fission source term and $\mathrm{BR}_{i\to j}$ the probability to decay from the nucleus i to the nucleus j. This equation can be written in a matrix form:

$$\frac{d\boldsymbol{N}(t)}{dt} = \boldsymbol{BLN}(t) + \boldsymbol{T} = \boldsymbol{AN}(t) + \boldsymbol{T} \tag{A2}$$

with

$$\boldsymbol{N} = \begin{bmatrix} N_0 \\ \vdots \\ N_n \end{bmatrix} \quad \boldsymbol{T} = \begin{bmatrix} \tau_0 \\ \vdots \\ \tau_n \end{bmatrix} \quad \boldsymbol{L} = \begin{bmatrix} \lambda_0 & & 0 \\ & \ddots & \\ 0 & & \lambda_n \end{bmatrix}$$

$$\boldsymbol{B} = \begin{bmatrix} -1 & & 0 \\ & \ddots & \\ \mathrm{BR}_{i\to j} & & -1 \end{bmatrix}$$

For each isotope i of the decay chain, the detected γ transition N_i^γ, during the measuring time Δt_m is written:

$$\begin{aligned}\forall i,\ N_i^\gamma(\Delta t_m) &= I_\gamma \epsilon_\gamma f_\gamma \int_0^{\Delta t_m} \lambda_i N_i(t)dt \\ \Leftrightarrow \frac{N_i^\gamma}{I_\gamma \epsilon_\gamma f_\gamma} &= \int_0^{\Delta t_m} \lambda_i N_i(t)dt = N_{d_i}(\Delta t_m)\end{aligned} \tag{A3}$$

with I_γ, ϵ_γ and f_γ the intensity, the detection efficiency and the sum effect correction factor respectively. If we define

$$\forall i,\ X_i(\Delta t_m) = \int_0^{\Delta t_m} N_i(t)dt \tag{A4}$$

Then,

$$\boldsymbol{N_d}(t) = \boldsymbol{LX}(t) \tag{A5}$$

Since the functions used are $\mathcal{C}^1$ class, we can integrate and switch the derivative and the integration of eq. (A2):

$$\frac{d\boldsymbol{X}(t)}{dt} = \boldsymbol{AX}(t) + t\boldsymbol{T} \tag{A6}$$

To make appear $\boldsymbol{N_d}(t)$, we need to multiplying eq. A6 by $\boldsymbol{L}$ and define $\boldsymbol{S} = \boldsymbol{LAL^{-1}}$:

$$\frac{d\boldsymbol{N_d}(t)}{dt} = \boldsymbol{SN_d}(t) + t\boldsymbol{LT} \tag{A7}$$

Here $\boldsymbol{S}$ is an inferior triangle matrix, we can then diagonalize it : $\boldsymbol{S} = \boldsymbol{RDR^{-1}}$. If we define $\boldsymbol{Y}(t) = \boldsymbol{R^{-1}N_d}(t)$ and $\boldsymbol{C} = \boldsymbol{R^{-1}LT}$ and multiply eq. A7 by $\boldsymbol{R^{-1}}$, it read:

$$\frac{d\boldsymbol{Y}(t)}{dt} = \boldsymbol{DY}(t) + t\boldsymbol{C} \tag{A8}$$

Since $\boldsymbol{D}$ is diagonal, we have n equations:

$$\forall i,\ \frac{dY_i(t)}{dt} = D_{ii}Y_i(t) + tC_i \tag{A9}$$

This is simply a first order differential equation with time dependant tC_i second member. With the bounding condition $Y_i(t=0) = 0$ (which means that there were no nucleus at time 0), C_i is written:

$$\forall i,\ C_i = \frac{D_{ii}^2}{e^{D_{ii}t} - 1 - D_{ii}t} Y_i(t) = E_{ii}(t)\, Y_i(t) \tag{A10}$$

Finally,

$$\begin{aligned}&\boldsymbol{T} = \boldsymbol{BN_d}(t) \ \text{ with } \boldsymbol{B} = \boldsymbol{L^{-1}RE}(t)\,\boldsymbol{R^{-1}} \\ &\text{and the diagonal matrix } \boldsymbol{E}(t) = \frac{\boldsymbol{D^2}}{\boldsymbol{e^{Dt} - 1 - Dt}}\end{aligned} \tag{A11}$$

Without a source term

Moreover, in the case of the background correction, the Bateman equation to resolve is:

$$\frac{d\boldsymbol{N}(t)}{dt} = \boldsymbol{A}\boldsymbol{N}(t) \tag{A12}$$

When integrating within a time t, we have:

$$\frac{d\boldsymbol{X}(t)}{dt} = \boldsymbol{A}\boldsymbol{X}(t) + \boldsymbol{M} \Leftrightarrow \frac{d\boldsymbol{N_d}(t)}{dt} = \boldsymbol{S}\boldsymbol{N_d}(t) + \boldsymbol{L}\boldsymbol{M} \tag{A13}$$

with $\boldsymbol{M}$ the unknown which is related to the initial number of nucleus. At the end, we have:

$$\begin{aligned} &\boldsymbol{M} = \boldsymbol{B}\boldsymbol{N_d}(t) \text{ with } \boldsymbol{B} = \boldsymbol{L^{-1}}\boldsymbol{R}\boldsymbol{E}(\boldsymbol{t})\boldsymbol{R^{-1}} \\ &\text{and the diagonal matrix } \boldsymbol{E}(t) = \frac{\boldsymbol{D}}{\boldsymbol{e^{Dt}-1}} \end{aligned} \tag{A14}$$

Analysis method and background correction

For the background correction, an additional step must be performed in order to assess the parameter $\boldsymbol{N_{d_{cont}}}$ which reflects the contribution of vacuum residual background on a new measurement. Figure 1 shows the origin of the background. In the time interval $t = [t_0, t_1]$ the background coming from the vacuum chamber is recorded $\boldsymbol{N_{d_{bkg}}}(t_1)$ and allows to determine $\boldsymbol{M}$. We suppose that there is no initial background ($\boldsymbol{N_d}(t = t_0) = 0$), then $N_{d_{bkg}}(t = t_0) = 0$:

$$\boldsymbol{N_{d_{bkg}}}(t_1) = \frac{N_i^{\gamma}(t_1)}{I_\gamma \epsilon_\gamma f_\gamma} \tag{A15}$$

The contribution from the background during the measurement in the time interval $t = [t_2, t_3]$ is:

$$\boldsymbol{N_{d_{cont}}} = \int_{t_2}^{t_3} \boldsymbol{L}\boldsymbol{N}(t)dt = \boldsymbol{N_d}(t_3) - \boldsymbol{N_d}(t_2) \tag{A16}$$

From eq. A5 and eq. A14, eq A16 is written:

$$\begin{aligned} \boldsymbol{N_{d_{cont}}} &= \left(\boldsymbol{B^{-1}}(t_3) - \boldsymbol{B^{-1}}(t_2)\right)\boldsymbol{M} \\ \boldsymbol{N_{d_{cont}}} &= \left(\boldsymbol{B^{-1}}(t_3) - \boldsymbol{B^{-1}}(t_2)\right)\boldsymbol{B}(t_1)\,N_{d_{bkg}}(t_1) \\ \boldsymbol{N_{d_{cont}}} &= \boldsymbol{R}\left(\boldsymbol{E^{-1}}(t_3) - \boldsymbol{E^{-1}}(t_2)\right)\boldsymbol{E}(t_1)\,\boldsymbol{R^{-1}}\boldsymbol{N_{d_{bkg}}}(t_1) \\ \Leftrightarrow \boldsymbol{N_{d_{cont}}} &= \boldsymbol{R}\left(\frac{\boldsymbol{e^{Dt_3}} - \boldsymbol{e^{Dt_2}}}{\boldsymbol{e^{Dt_1}-1}}\right)\boldsymbol{R^{-1}}\boldsymbol{N_{d_{bkg}}}(t_1) \end{aligned} \tag{A17}$$

* abdelhazize.chebboubi@cea.fr

[1] O. Hahn and F. Strassmann, Naturwissenschaften **27**, 11 (1939).
[2] L. Meitner and O. R. Frisch, Nature **143**, 239 (1939).
[3] H. Goutte, J. F. Berger, P. Casoli, and D. Gogny, Phys. Rev. C **71**, 24316 (2005).
[4] P. Möller, A. J. Sierk, and A. Iwamoto, Phys. Rev. Lett. **92**, 72501 (2004).
[5] J. Randrup and P. Möller, Phys. Rev. Lett. **106**, 132503 (2011).
[6] E. Torleif, Adv. Phys. **9**, 425 (1960).
[7] P. Fong, Phys. Rev. **102**, 434 (1956).
[8] B. D. Wilkins, E. P. Steinberg, and R. R. Chasman, Phys. Rev. C **14**, 1832 (1976).
[9] J. R. Nix and W. J. Swiatecki, Nucl. Phys. **71**, 1 (1965).
[10] Y. Aritomo, S. Chiba, and F. Ivanyuk, Physical Review C **90**, 054609 (2014).
[11] A. Chebboubi, G. Kessedjian, O. Litaize, O. Serot, H. Faust, D. Bernard, A. Blanc, U. Köster, O. Méplan, P. Mutti, and C. Sage, Physics Letters B **775**, 190 (2017).
[12] J. Kaufmann, W. Mollenkopf, F. Gönnenwein, P. Geltenbort, and A. Oed, Zeitschrift für Physik A Hadrons and Nuclei **341**, 319 (1992).
[13] U. Quade, K. Rudolph, S. Skorka, P. Armbruster, H.-G. Clerc, W. Lang, M. Mutterer, C. Schmitt, J. Theobald, F. Gönnenwein, J. Pannicke, H. Schrader, G. Siegert, and D. Engelhardt, Nuclear Physics A **487**, 1 (1988).
[14] N. Boucheneb, P. Geltenbort, M. Asghar, G. Barreau, T. Doan, F. Gönnenwein, B. Leroux, A. Oed, and A. Sicre, Nuclear Physics A **502**, 261 (1989).
[15] P. Armbruster, M. Asghar, J. P. Bocquet, R. Decker, H. Ewald, J. Greif, E. Moll, B. Pfeiffer, H. Schrader, F. Schussler, G. Siegert, and H. Wollnik, Nucl. Instrum. Methods **139**, 213 (1976).
[16] U. Köster, H. Faust, T. Materna, and L. Mathieu, Nucl. Instrum. Meth. A **613**, 363 (2010).
[17] G. Fioni, H. R. Faust, M. Gross, M. Hesse, P. Armbruster, F. Gönnenwein, and G. Münzenberg, Nucl. Instrum. Meth. A **332**, 175 (1993).
[18] F. Martin, *Etude des distributions en masse, charge nucléaire et énergie cinétique des produits de fission de l'233U(nth,f) et du 241Pu(nth,f) mesurées auprès du spectromètre de masse Lohengrin (ILL)*, Ph.D. thesis, Université de Grenoble (2013).
[19] A. Chebboubi, *Contribution à l'étude de la fission nucléaire : de LOHENGRIN à FIPPS*, Ph.D. thesis, Université Grenoble Alpes (2015).
[20] S. Julien-Laferriere, *Approche expérimentale et phénoménologique des rendements de la fission induite par neutron thermique du 239Pu et du 241Pu*, Ph.D. thesis, Université Grenoble Alpes (2018).
[21] S. Julien-Laferrière, A. Chebboubi, G. Kessedjian, and O. Serot, EPJ Nuclear Sciences & Technologies **4**, 25

(2018).
[22] Y. Gupta, D. Biswas, O. Serot, D. Bernard, O. Litaize, S. Julien-Laferrière, A. Chebboubi, G. Kessedjian, C. Sage, A. Blanc, H. Faust, U. Köster, A. Ebran, L. Mathieu, A. Letourneau, T. Materna, and S. Panebianco, Physical Review C **96** (2017), 10.1103/PhysRevC.96.014608.
[23] J. Theuerkauf, S. Esser, S. Krink, M. Luig, N. Nicolay, O. Stuch, and H. Wolters, *Program Tv*, Tech. Rep. (Institute for Nuclear Physics, Cologne, 1993).
[24] Y. Khazov, A. A. Rodionov, S. Sakharov, and B. Singh, Nucl. Data Sheets **104**, 497 (2005).
[25] S. Sudár, *Contract*, Tech. Rep. (Institute of Experimental Physics, University of Debrecen, 2009).
[26] M. Chadwick, M. Herman, P. Obložinský, M. Dunn, Y. Danon, A. Kahler, D. Smith, B. Pritychenko, G. Arbanas, R. Arcilla, R. Brewer, D. Brown, R. Capote, A. Carlson, Y. Cho, H. Derrien, K. Guber, G. Hale, S. Hoblit, S. Holloway, T. Johnson, T. Kawano, B. Kiedrowski, H. Kim, S. Kunieda, N. Larson, L. Leal, J. Lestone, R. Little, E. McCutchan, R. MacFarlane, M. MacInnes, C. Mattoon, R. McKnight, S. Mughabghab, G. Nobre, G. Palmiotti, A. Palumbo, M. Pigni, V. Pronyaev, R. Sayer, A. Sonzogni, N. Summers, P. Talou, I. Thompson, A. Trkov, R. Vogt, S. van der Marck, A. Wallner, M. White, D. Wiarda, and P. Young, Nuclear Data Sheets **112**, 2887 (2011).
[27] A. Santamarina, D. Bernard, P. Blaise, M. Coste, A. Courcelle, T. Huynh, C. Jouanne, P. Leconte, O. Litaize, S. Mengelle, G. Noguère, J.-M. Ruggiéri, O. Serot, J. Tommasi, C. Vaglio, and J.-F. Vidal, *The JEFF-3.1.1 Nuclear Data Library*, Tech. Rep. (NEA, 2009).
[28] O. Litaize and O. Serot, Physical Review C **82**, 054616 (2010).
[29] O. Litaize, O. Serot, and L. Berge, The European Physical Journal A **51**, 177 (2015).
[30] D. Regnier, O. Litaize, and O. Serot, Computer Physics Communications **201**, 19 (2016).
[31] K.-H. Schmidt, B. Jurado, C. Amouroux, and C. Schmitt, Nuclear Data Sheets **131**, 107 (2016).
[32] R. Capote, M. Herman, P. Obložinský, P. Young, S. Goriely, T. Belgya, A. Ignatyuk, A. Koning, S. Hilaire, V. Plujko, M. Avrigeanu, O. Bersillon, M. Chadwick, T. Fukahori, Z. Ge, Y. Han, S. Kailas, J. Kopecky, V. Maslov, G. Reffo, M. Sin, E. Soukhovitskii, and P. Talou, Nuclear Data Sheets **110**, 3107 (2009).
[33] M. Verpelli and R. Capote, International Nuclear Data Committee INDC(NDS)-0702 (2015).
[34] A. Gilbert and A. G. W. Cameron, Can. J. Phys. **43**, 1446 (1965).
[35] F. Bečvář, Nuclear Instruments and Methods in Physics Research Section A: Accelerators, Spectrometers, Detectors and Associated Equipment **417**, 434 (1998).
[36] A. Koning and J. Delaroche, Nuclear Physics A **713**, 231 (2003).
[37] J. Raynal, *Notes on ECIS94*, Tech. Rep. (CEA, Saclay, 1994).
[38] J. Kopecky and M. Uhl, Phys. Rev. C **41**, 1941 (1990).
[39] T. Kibédi, T. Burrows, M. Trzhaskovskaya, P. Davidson, and C. Nestor, Nuclear Instruments and Methods in Physics Research Section A: Accelerators, Spectrometers, Detectors and Associated Equipment **589**, 202 (2008).
[40] L. Landau, in *Collected Papers of L. D. Landau* (1965).
[41] A. Chebboubi, O. Serot, G. Kessedjian, O. Litaize, A. Blanc, D. Bernard, H. Faust, S. Julien-Laferrière, U. Köster, A. Letourneau, T. Materna, O. Méplan, P. Mutti, M. Rapala, and C. Sage, in *EPJ Web of Conferences*, Vol. 146 (2017).
[42] T. Wang, G. Li, L. Zhu, Q. Meng, L. Wang, H. Han, W. Zhang, H. Xia, L. Hou, R. Vogt, and J. Randrup, Physical Review C **93**, 014606 (2016).
[43] M. Jandel, B. Baramsai, T. Bredeweg, A. Couture, A. Favalli, A. Hayes, K. Ianakiev, M. Iliev, T. Kawano, S. Mosby, G. Rusev, I. Stetcu, P. Talou, J. Ullmann, D. Vieira, C. Walker, and J. Wilhelmy, Nuclear Instruments and Methods in Physics Research Section A: Accelerators, Spectrometers, Detectors and Associated Equipment **882**, 105 (2018).
[44] C. Michelagnoli, A. Blanc, E. Ruiz-Martinez, A. Chebboubi, H. Faust, E. Froidefond, G. Kessedjian, M. Jentschel, U. Köster, P. Mutti, and G. Simpson, EPJ Web of Conferences **193**, 04009 (2018).

Fission fragments observables measured at the LOHENGRIN spectrometer

S. Julien-Laferrière[1,2], *L.* Thombansen[2], *G.* Kessedjian[2], *A.* Chebboubi[1], *O.* Serot[1], *C.* Sage[2,*], *O.* Méplan[2], *M.* Ramdhane[2], *O.* Litaize[1], *J.* Nicholson[1], *D.* Bernard[1], *U.* Köster[3], *P.* Mutti[3], *T.* Materna[4], and *M.* Rapala[4]

[1]CEA, DEN, DER, SPRC, LEPh, Cadarache center, F-13108 Saint-Paul-lez-Durance, France
[2]LPSC, Université Grenoble-Alpes, CNRS/IN2P3, F-38026 Grenoble Cedex, France
[3]Institut Laue-Langevin, F-38042 Grenoble Cedex 9, France
[4]CEA, DSM, IRFU, SPhN, LEARN, Saclay center, F-91191 Gif-sur-Yvette, France

Abstract. Nuclear fission yields are key data for reactor studies, such as spent fuel inventory or decay heat, and for understanding fission process. Despite a significant effort allocated to measure fission yields during the last decades, the recent evaluated libraries still need improvements in particular in the reduction of the uncertainties. Moreover, some discrepancies between these libraries must be explained.
Additional measurements provide complementary information and estimations of experimental correlations, and new kinds of measurements enable to test the models used during the nuclear data evaluation process. A common effort by the CEA, the LPSC and the ILL aims at tackling these issues by providing precise measurements of isotopic and isobaric fission yields with the related variance-covariance matrices. Additionally, the experimental program involves a large range of observables requested by the evaluations, such as kinetic energy dependency of isotopic yields and odd-even effect in order to test the sharing of total excitation energy and the spin generation mechanism. Another example is the complete range of isotopic distribution per mass that allows the determination of the charge polarization, which has to be consistent for complementary masses (pre-neutron emission). For instance, this information is the key observable for the evaluation of isotopic yields. Finally, ionic charge distributions are indirect measurements of nanosecond isomeric ratios as a probe of the nuclear de-excitation path in the (E^*, J, π) representation.
Measurements for thermal neutron induced fission of ^{241}Pu have been carried out at the ILL in Grenoble, using the LOHENGRIN mass spectrometer. Methods, results and comparison to models calculations will be presented corresponding to a status on fission fragments observables reachable with this facility.

1 Introduction

An accurate knowledge of fission data in the actinide region is important for studies of innovative nuclear reactor concepts. Fission yield measurements supply experimental data to put constraints on fission models and improve their predictive power. In the framework of nuclear data evaluation, these models are indeed necessary to increase the consistency and the precision of the libraries. Despite a real effort on fission yields measurements, current evaluated data still need some improvements on different aspects, such as for instance the uncertainties reduction and the estimation of covariance matrices. A special focus on the heavy and symmetry mass regions is important, since it is where the discrepancies between models (or evaluations) and the few experimental data are mainly observed.

A collaboration between the CEA, the LPSC and the Institute Laue Langevin (ILL) is involved in an experimental program using thermal neutrons of the ILL and the LOHENGRIN spectrometer to study the fission process. We developed different methodologies to obtain absolute isobaric and isotopic yields with the estimation of the covariance matrices associated to the measurements. Besides, the measurement of different observables combined with a comparision with simulation codes such as FIFRELIN [1] enable to get insight data to better understand the fission process. Isomeric ratios can give an indirect information on the fragments spin ditribution, and their kinetic energy dependency enlights on the validity of the models in use. An exhaustive set of isotopic yields per mass enables the charge polarisation estimation, which has to be consistent between complementary masses. A final example of such indirect data measured by our collaboration is the extraction of nanosecond isomeric ratios determined from the ionic charge distributions per isotope.

*e-mail: sage@lpsc.in2p3.fr

2 The LOHENGRIN spectrometer

The LOHENGRIN mass spectrometer [2] is a nuclear physics instrument from the ILL research reactor facility which allows to study fragment distributions from thermal neutron induced fission with a very high mass resolution ($\Delta A/A \approx 1/400$). A fissile actinide target is placed close to the reactor core, in a thermal neutron flux reaching 5×10^{14} neutron.cm^{-2}.s^{-1}.

Fission fragments emerge from the target with an ionic charge distributed around an average ionic charge state of

about 20 to 23. Those fragments that are emitted along the beam tube axis undergo a horizontal deflection in a magnetic field, directly followed by a vertical deflection in an electric field. These combined fields separate ions according to their A/q and E_k/q ratios, with A, q and E_k the mass, ionic charge state and kinetic energy of the ions respectively. These ratios can be achieved with different triplets (A, E_k, q) leading to a possible degeneracy.

At the spectrometer exit, different detection systems can be installed, such as a dual anode Frisch grid ionisation chamber for mass yield measurements, or two clovers of four high purity Germanium crystals that are used with an additional magnet whose aim is to focus the ion beam. A schematic view of the spectrometer is shown in Fig. 1.

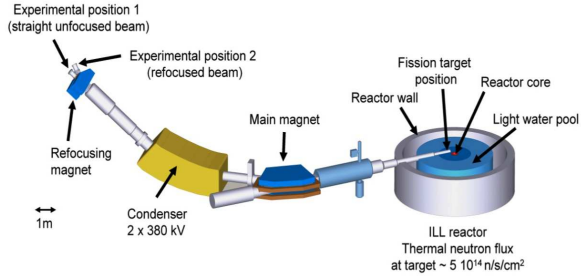

Figure 1. Schematic overview of the LOHENGRIN spectrometer at ILL.

3 Mass and isotopic yields measurements of the ^{241}Pu(n$_{th}$,f) reaction

The first goal of our collaboration measurement campaign consists in the precise measurements of mass, isotopic and isomeric yields, with a control of the systematic effects and the determination of the covariance matrices associated to the analyses. For these observables, their dependency with fission fragment kinetic energy increases significantly the retrieved information on the fission process.

3.1 Mass yields

Isobaric yields are obtained from experimental position 1 (see Fig. 1) after an integration over the kinetic energy and the ionic charge distributions of the count rates measured with the ionisation chamber. A new measurement method and consequent analysis path have been developed and are detailed in Ref. [3–6]. Among the special features of this method are the self-normalisation of our data and the calculation of the experimental covariance matrices. Provided that all the heavy mass rates are measured, it is possible to self-normalise the data by defining to 100% the sum of the whole heavy peak yields. As a consequence, these new measurements are independent from another experiment or assessment and may be compared directly with the existing data and evaluations.

The results for ^{241}Pu(n$_{th}$,f) are shown in Fig. 2, where they are compared to the JEFF-3.3 [7] and ENDF/B-VII.1 [8] libraries. The whole heavy peak and an important part of the light one were measured. Our results are slightly higher than the libraries for the light mass region, and a structure around mass 140 is observed in the heavy region. Our experimental uncertainties are around 5% on average and below the ones indicated in the two libraries.

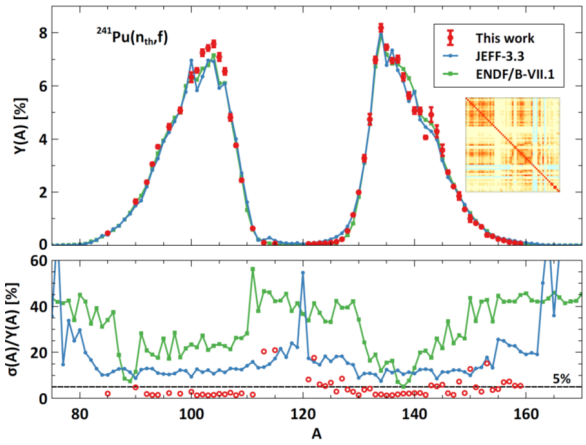

Figure 2. Mass yields for the ^{241}Pu(n$_{th}$,f) reaction and their relative uncertainties.

3.2 Isotopic yields

Isotopic and long-lived isomeric (few μs to ms) fission yields are measured by gamma spectrometry. Experimental position 2 (see Fig. 1) is now used.The ion beam is deposited on a moving tape inside a vacuum chamber and a cumulative measurement with duration of about 30 min per point over the ionic charge distribution is achieved. The tape moves at the end of the measurement to clean the environment and start a new measurement. After corrections of the Bateman equations and the estimation of the contribution of the isotopes from the tape only, we obtain the isotopic distributions per mass. As for the mass yields, a particular effort is made on the determination of the systematic uncertainties and the covariance associated to the measurement process.

Fig. 3 shows a scheme summarizing the measurement procedure and the isotopic yields obtained for the chains 137 and 139 are shown in Fig. 4, along with the covariance matrices. It is important to note that the uncertainties are dominated by the nuclear structure data. Thus current yields measurements can be improved by increasing the nuclear structure knowledge. Fig. 5 helps to understand the construction of the experimental covariance matrix at the main steps of the analysis as illustration of the uncertainty propagation effects.

4 Indirect data measurements

Besides isobaric and isotopic yields, other fission observables are achievable with the LOHENGRIN spectrometer and give important complementary information for the study of the fission process. The kinetic energy dependency of the isotopic and isomeric yields has been already

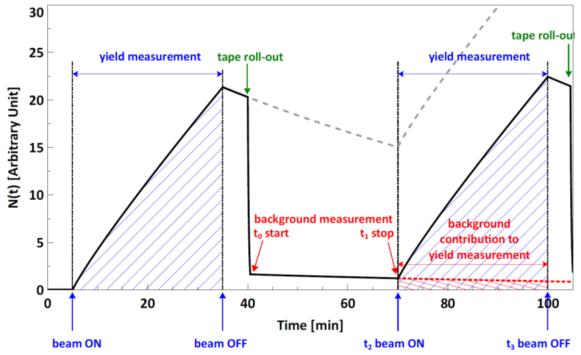

Figure 3. Evolution of a typical isotopic yields measurement procedure.

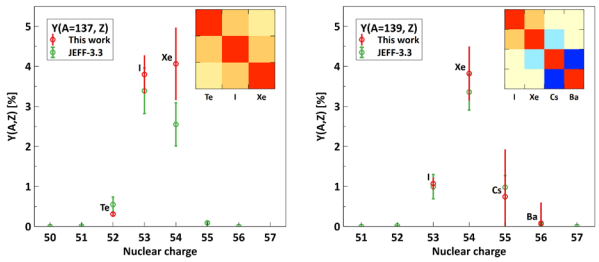

Figure 4. Isotopic yields of the ^{241}Pu(n$_{th}$,f) reaction for masses 137 and 139, along with the experimental covariance matrices

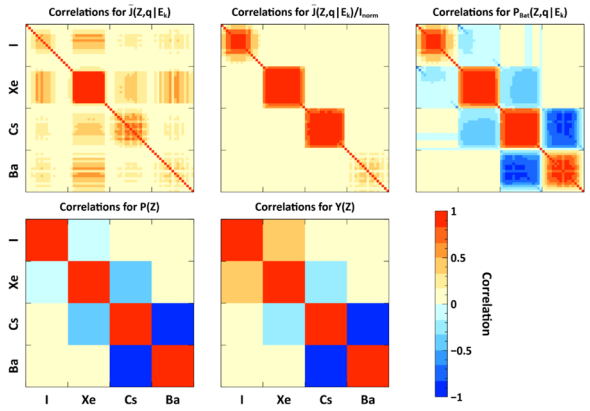

Figure 5. The correlation matrix for mass 139 at different steps of the analysis. 1st step: average on the different gamma rays. 2nd step: Division by I^{norm}. 3rd step: Independent production rate calculation. 4th step: sum over the ionic charges. 5th step: absolute yields after self normalisation.

discussed in ref. [9, 10]. This paper will focus on the description of the charge polarisation and the estimation of nanosecond isomeric ratios.

4.1 Nuclear charge polarisation

The charge polarisation can be extracted from the combination of the isotopic and isobaric yields measurements. It is defined as the difference between the measured mean nuclear charge and the fragment nuclear charge in the Unchanged Charge Density (UCD) hypothesis.

Fig. 6 shows the measured charge polarisation for the concerned masses in the heavy peak region, compared with the JEFF-3.1.1 library and previous experimental data from Schillebeeckx et al. [11]. We observe a good agreement for the mass 130 and around mass 140, but a strong structure appears for the masses 132, 136 and 138. Complementary measurements on the neighbouring masses are planned by the collaboration to better understand this phenomenon.

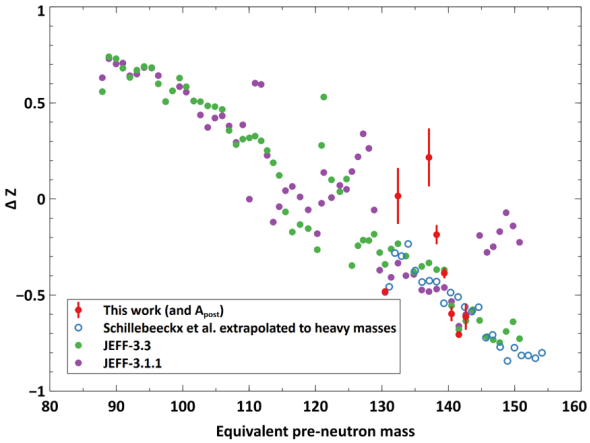

Figure 6. Charge polarisation measured in the heavy peak region as a function of the pre-neutron mass, compared with the JEFF-3.1.1 library and previous experimental data from Schillebeeckx et al. [11].

4.2 Nanosecond converted isomeric ratios

Indirect measurements of nanosecond IR's can be determined from the ionic charge distributions [12, 13]. The method consists in the deconvolution of the ionic charge distribution per isotope obtained by gamma spectrometry after correction from Bateman equations. The converted isomeric ratio (CIR) is defined as the converted isomer population over the total ionic population (converted and unconverted).

$$CIR = \frac{N(A,Z,m \rightarrow e^-)}{N(A,Z,GS) + N(A,Z,m \rightarrow \gamma) + N(A,Z,m \rightarrow e^-)} \quad (1)$$

According to the statistical models from H. Betz [14], we assume that the ionic charge distribution associated to the unconverted population follows a Gaussian distribution due to the charge equilibrium in the cover of the target (a Nickel foil in this work). A deviation from this Gaussian distribution indicates a charge modification due to the conversion from ps and ns isomers to groundstate (see Fig. 7). In most of the cases the deconvolution is achieved using two Gaussian distributions and a Monte Carlo simulation to deduce the CIR in order to consider the covariance terms between the Gaussian integrals. CIR measurements for ^{241}Pu(n$_{th}$,f) and ^{233}U(n$_{th}$,f) are shown in Fig. 8 and compared to FIFRELIN calculations for ^{241}Pu(n$_{th}$,f). We note

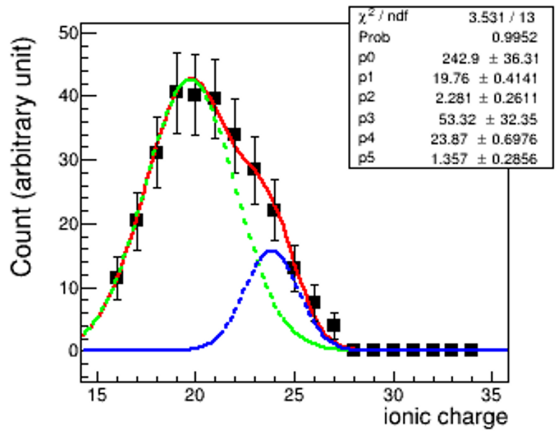

Figure 7. Ionic charge distribution de-convoluted using the Gaussian assumption for the unconverted state according to the Betz model [14]. The blue curve corresponds to the ns isomer contribution.

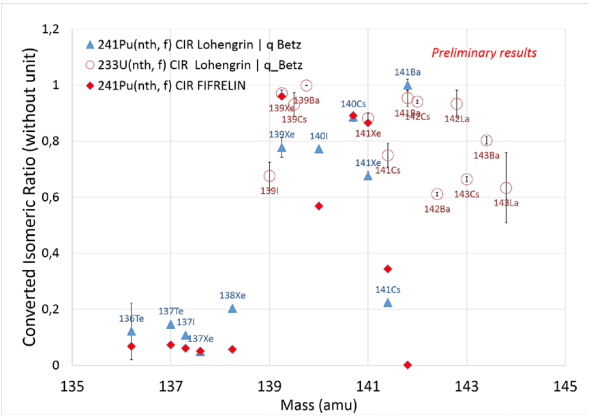

Figure 8. Converted isomeric ratios as a function of the mass induced by the fission of $^{241}Pu(n_{th},f)$ and $^{233}U(n_{th},f)$ in comparison with FIFRELIN calculations.

a good tendency even if some differences have to be explored in details given the assumption used in the analysis or the models considered for the decay cascade calculations. For some nuclei, many isomers and bands have to be taken into account at the limit of the knowledge of the nuclear structure. Then it corresponds to integral measurements used to test the overal decay cascade.

5 Conclusion and perspectives

An experimental program dedicated to precise absolute measurements of isobaric, isotopic and isomeric yields is ongoing using the LOHENGRIN mass spectrometer at ILL. Recent results concern the $^{241}Pu(n_{th},f)$ reaction, where a dedicated analysis method with a control of the systematic uncertainties and computation of the covariance matrices was achieved. Interesting indirect data are also measured and dedicated to test the phenomenological models and the assumptions used for the evaluations, through a comparison with calculations using the FIFRELIN code developped at CEA Cadarache. In this frame, nuclear charge polarisation and nanosecond CIR are the main examples of such investigations. Our collaboration plans to continue this measurement program for different fissioning systems, as new measurements and validated models are central in order to progress in the evaluation topic.

Acknowledgements

This work was supported by CEA, IN2P3 and "le défi NEEDS". The authors are grateful for the support of the ILL and all the staff involved from CEA Cadarache and LPSC.

References

[1] O. Litaize and O. Serot, Eur. Phys. J . A **51**, 177 (2015)
[2] P. Armbruster *et al.*, *Nucl. Instrum. Methods* **139** 213 (1976)
[3] F. Martin *et al.*, Proc. 2nd ANIMMA Conference, June 2011, Ghent (Belgium).
[4] F. Martin *et al.*, Nuclear Data Sheets **119**, 328-330 (2014)
[5] S. Julien-Laferrière *et al.*, EPJ Nucl. Sci. Technol. **4**, 25 (2018)
[6] Y. Gupta *et al.*, Phys. Rev. C **96**, 014608 (2017)
[7] The JEFF-3.1.1 nuclear data library. OECD, NEA, JEFF Report 21, ISBN 92-64-02314-3 (2006).
[8] M. B. Chadwick *et al.*, Nucl. Data Sheets **107**, 2931 (2006)
[9] S. Julien-Laferrière *et al.*, EPJ Web of Conferences **211**, 04004 (2019)
[10] A. Chebboubi *et al.*, Phys. Lett. B **775**, 190-195 (2017)
[11] P. Schillebeeckx *et al.*, Nucl. Phys. A **580**, 15-32 (1994)
[12] T. Rzaca-Urban, J. Genevey, T. Materna *et al.*, Phys. Rev. C **80**, 064317 (2009)
[13] A. Chebboubi *et al.*, EPJ Web of Conferences **146**, 04021 (2017)
[14] H. D. Betz, Rev. Mod. Phys. **44**, 465-539 (1972)
[15] R. Capote *et al.*, Nucl. Data Sheets **110**, 3107 (2009)

Investigation of fission product isomeric ratios and angular momenta of ^{132}Sn populated in the ^{241}Pu(n_{th},f) reaction

Jehaan Nicholson[1], *Abdelhazize* Chebboubi[1,*], *Olivier* Serot[1], *Grégoire* Kessedjian[2], *Yung Hee* Kim[3], *Ulli* Köster[3], *Olivier* Litaize[1], *Olivier* Méplan[2], and *Christophe* Sage[2], and *Mourad* Ramdhane[2]

[1]CEA, DEN, DER, SPRC, Cadarache, Physics Studies Laboratory, 13108 Saint-Paul-lès-Durance, France
[2]LPSC, Université Grenoble-Alpes, CNRS/IN2P3, 38026 Grenoble Cedex, France
[3]Institut Laue-Langevin, 38042 Grenoble Cedex 9, France

Abstract. During an experimental campaign performed at the LOHENGRIN recoil spectrometer of the Institut Laue-Langevin (ILL), a kinetic energy dependence of ^{132}Sn fission product isomeric ratio (IR) has been measured by inducing thermal fission of ^{241}Pu. The IRs are deduced using gamma ray spectrometry in coincidence with the ionisation chamber. To interpret these data, we use the FIFRELIN Monte-Carlo code to simulate the de-excitation of the fission fragments. Combining the IRs with the FIFRELIN calculations, the angular momentum distribution with kinetic energy of the doubly magic nucleus of ^{132}Sn was deduced. This will be compared with the angular momentum distribution obtained for the reaction ^{235}U(n_{th},f) for ^{132}Sn.

1 Introduction

The past decade has seen a growing energy need and thus a renewed interest in nuclear energy. Nonetheless, to make the new reactors more safe, the existing technology needs to be improved and the challenge for new and innovative fuel must be overcome. Furthermore, a precise understanding of the fission process is a noteworthy challenge faced by nuclear physicists even though eight decades have passed since its discovery in 1939 [1, 2]. Many different models and hypotheses such as the liquid drop model, shell model etc. have been developed to explain and reproduce the experimental data obtained as well as to improve the understanding of fission. However, the angular momenta of the fission fragments are a poorly known quantity. Angular momenta of fission fragments are a component of the phenomenological model used to assess nuclear observables used in applications as prompt gammas and neutrons. This angular momentum can be estimated by using models, see for example Ref. [3], or through direct measurements, see Ref. [4] and references therein. On the other hand, one can study indirectly the angular momenta of the fission fragments by measuring the isomeric ratios of the fission fragments [5–7].

*e-mail: Abdelhazize.CHEBBOUBI@cea.fr

2 Experiment

The experiment was conducted at the LOHENGRIN recoil spectrometer [8] at the Institut Laue-Langevin (ILL) [9]. The LOHENGRIN recoil spectrometer was built in the 1970s and is one of the key instruments at the ILL to carry out experiments for nuclear physics and nuclear data. The LOHENGRIN recoil spectrometer enables us to study the mass, charge and kinetic energy distribution of the fission products. These fission products are obtained by exposing a fissile or fertile target to a thermal neutron flux of about 5×10^{14} n/cm^2/s near the core of the ILL high-flux reactor. The total length of LOHENGRIN is 23 m and has a high mass resolution (A/ΔA ≅400) [10], which is dependent on target size. By using the electric and magnetic fields of LOHENGRIN, fission products of interest are extracted and brought to the detection area. These fields are perpendicular to each other and have focussing properties in their respective planes.

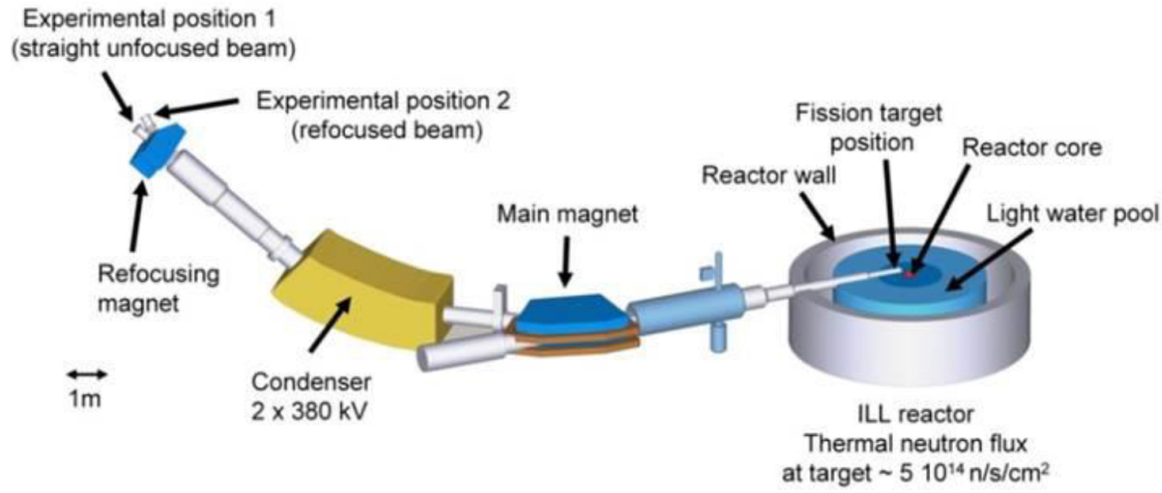

Figure 1. Schematic of the LOHENGRIN mass spectrometer showing the dipole magnet in blue (centre) and the electrostatic condenser in yellow. They are used to generate the electric and magnetic fields, which are used to select and divert the charged fission products.

For this experiment, we used ^{241}Pu (39.9 μg/cm^2) as the target nuclei. By varying the electric and magnetic fields, the desired fission products are selected by the A/q and E_k/q ratio, where A is the desired mass of the fission product, q is the ionic charge and E_k its kinetic energy. As can be seen from Fig. 1, there are two experimental positions present. At experiment position 1, the beam has an energy dispersion of 7.2 cm per 1% energy difference, whereas at position 2, the beam is refocussed in the energy axis using the RED magnet [11] and, hence, the particle flux density is increased by up to a factor of seven [10] as compared to position 1. In our experiment, the detectors were set up at position 2. The detection setup consists of an ionisation chamber and two HPGe clover detectors with four germanium crystals each. This is depicted in Figure 2.

The extracted fission products are then implanted in the Al foil at the top of the ionisation chamber. The gamma rays, emitted by internal transition (IT) of the isomeric state and after the β- decay of the ground state are detected using the two clover detectors. By using LOHENGRIN, ^{132}Sn was extracted at ionic charges 20 and 24 respectively with kinetic energy ranging from 57 MeV to 84 MeV.

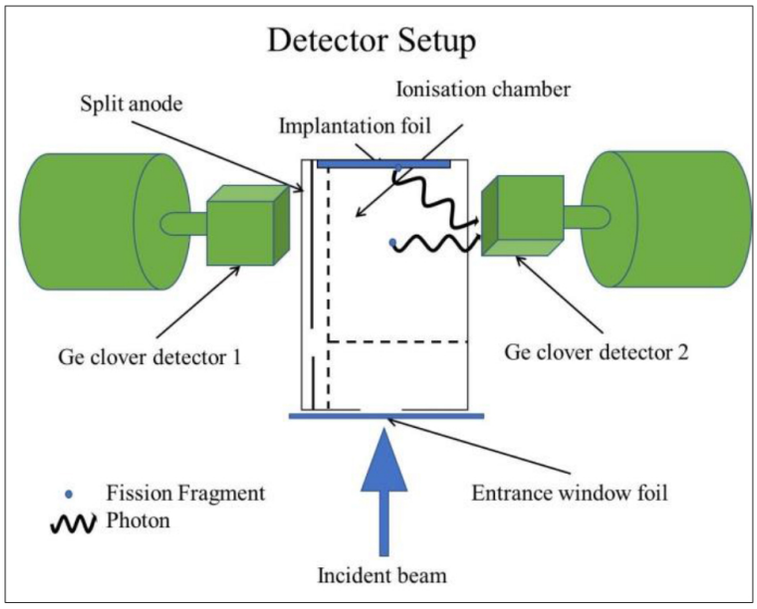

Figure 2. Detector setup showing the two HPGe clover detectors in green and the split-anode ionisation chamber in between them. The implantation foil is placed at the top of the ionisation chamber to trap the fission products.

3 Isomeric ratios from experiments

Isomeric ratios (IR) are defined as ratio of the production rate (P_i) of one isomeric state to the sum of the production rates of all the isomeric states and the ground state (GS).

$$IR = \frac{P_i}{\sum P_i + GS} \tag{1}$$

3.1 The analysis

^{132}Sn has one microsecond isomeric state at 4848.5 keV having $J^{\pi} = 8^{+}$ with a half-life of 2.08 μs [12]. The analysis was carried out off-line. To analyse the gamma rays originating from the isomeric state, a coincidence spectrum was generated. The time coincidence window was set to 20 μs. The coincidence was created between the ionisation chamber and the HPGe clover detectors. By using the coincidence method to generate a spectrum, we are able to reduce the gammas originating from room background and beta decays and gammas from β- decay of the ground state of the parent nucleus (^{132}In). Thus, we obtain a clean spectrum for the gamma rays originating from the microsecond isomeric state of ^{132}Sn as seen in the Fig. 3. For the measurement of the gamma rays originating from the β- decay of the ground state (^{132}Sn), the ungated spectrum was used.

The gamma spectrum was analysed using the TV gamma spectrum analyser program [13]. The intensities of the gamma rays were obtained from literature [12] and the efficiencies for the germanium detectors were obtained from simulations validated with experimental data. To calculate the IR from the counts obtained from the gamma spectra, firstly, we have to calculate the production rates of the isomeric state as well as the ground state. To do this, the Bateman equations need to be solved. Along with this, corrections for the decay during flight also need to be taken into account; this is due to the fact that the distance between target and the experimental focal plane is 23 m. To accurately determine the production rates and the IR along with their respective uncertainties, a Monte-Carlo method [5, 14] is being used. This

Monte-Carlo Code (MCC) is used as compared to the analytical method as there are quite a few parameters involved in different corrections, which need to be added. Hence trying to propagate and calculate their uncertainties analytically would be a complex task.

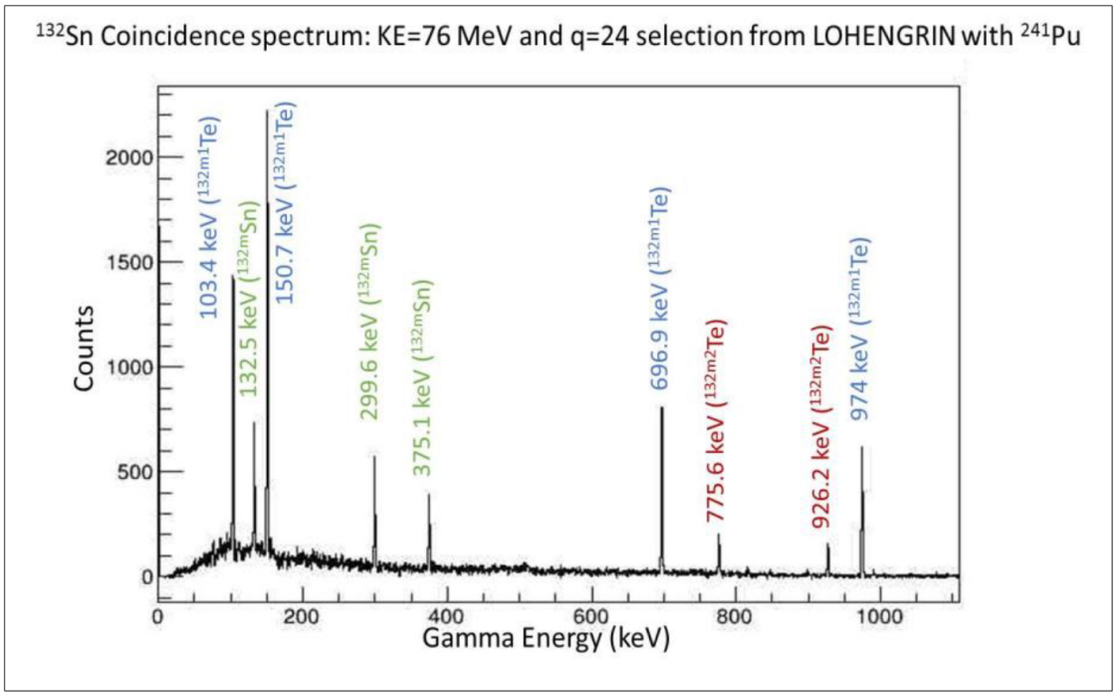

Figure 3. Gated Spectrum showing the three gamma rays of interest (in green) from the ^{132}Sn isomeric state (IS). Gamma rays from the two ISs of ^{132}Te are also observed in this spectrum.

As input to the MCC, one must provide the half-life of the states (ground and isomeric), counts and the error on counts which are extracted using TV gamma spectrum analyser, detection efficiency, the gamma intensities and the normalisation factor for the gamma intensities, the branching ratio, kinetic energy selected by LOHENGRIN and the flight path length. The MCC then calculates the average number of disintegrations (N_d), the production rates and the isomeric ratios along with their respective uncertainties. One can also obtain sensibility plots as well as covariance matrices from the MCC.

In the MCC, N_d is calculated for each of the gamma rays (N_{di}) arising from a particular state, these N_{di} are then used to calculate the mean N_d. The χ^2 test is used to verify whether a 90% level of confidence is achieved. If not, progressively, uncertainty is added [15] and the N_d is recalculated to achieve the test criteria. Thus, a final mean value of the N_d along with its uncertainty is obtained. The systematic uncertainties account for less than 5%, whereas the statistical uncertainties go as high as 50%.

The beamtime had a span of ten days and hence, not all the measurements were performed consecutively or even on the same day. For this reason, we must take into account the target evolution. To see the target evolution, several energy scans were carried out throughout the experiment schedule. The shift in the mean value of the kinetic energy between the first and the last experimental days is equal to (4.6 ± 1.0) MeV. It should be noted that the evolution of the mean kinetic energy was linear with a slope of (−0.52 ± 0.09) MeV/day. For each kinetic energy selected with the LOHENGRIN spectrometer, IRs are measured. By combining all the experimental data (weighted by the kinetic energy distribution) the mean IR can be derived and is equal to 0.0719 ± 0.0016. It should be noted that covariance was not taken into account for the uncertainty propagation.

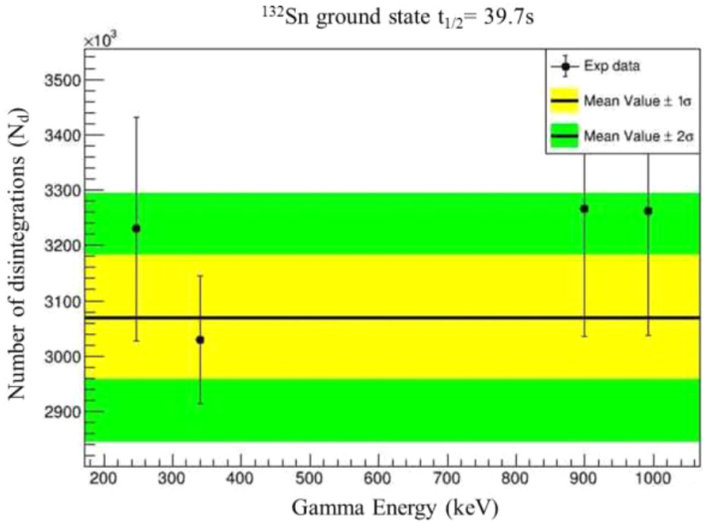

Figure 4. Number of disintegrations calculation using the MCC for GS for 72 MeV and q=24 selection of LOHENGRIN.

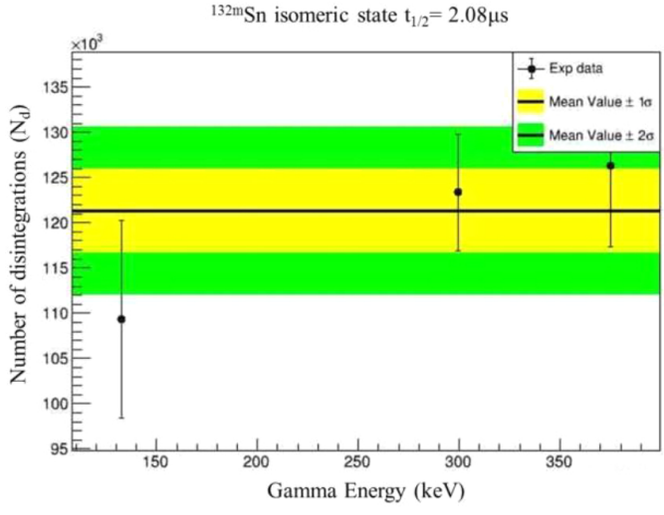

Figure 5. Number of disintegrations calculation using the MCC for IS for 72 MeV and q=24 selection of LOHENGRIN.

4 Spin extraction using FIFRELIN

FIssion FRagment Evaporation Leading to an Investigation in Nuclear data (FIFRELIN) [16] is a Monte-Carlo code developed at CEA. This code simulates the fission process and gives information on fission observables such as prompt neutrons, gammas, neutron multiplicity. For this work, this code has only been used to carry out the de-excitation simulation of the nuclei of interest (^{132}Sn). The inputs provided for this code are the mass number (A), the atomic number (Z), excitation energy (E^*) and spin along with parity (J^π). It also requires additional files from the RIPL-3 2015 [17, 18] library to get information on the nuclear levels and the gammas and electrons emitted at lower energies. Additional models are also required such as the Composite Gilbert-Cameron Model (CGCM), which is propositioned in RIPL-3 [17] for nuclear level densities, Back Shifted Fermi Gas Model (BSFGM) for spin cut-off and the Enhanced General Lorentzian (EGLO) model [19] for the gamma strength functions. The BRICC code [20] is used to calculate the internal conversion coefficients. FIFRELIN

uses these input libraries and assumes that the experimental level scheme provided in the RIPL-3 2015 file is complete up to cut-off energy (E_{cut}). After this E_{cut}, it is assumed that the experimental level scheme is incomplete and this is then filled by FIFRELIN using the CGCM model. The BSFGM is used to attribute a J^{π} value to these new levels and the EGLO model is used to get the gammas and their respective intensities originating from these levels. The probability to emit neutrons are obtained from the neutron transmission coefficients which are derived from an optical model; the Koning-Delaroche global neutron optical model potential [21] but in our case, no neutrons are emitted as the simulations were run below neutron separation energy.

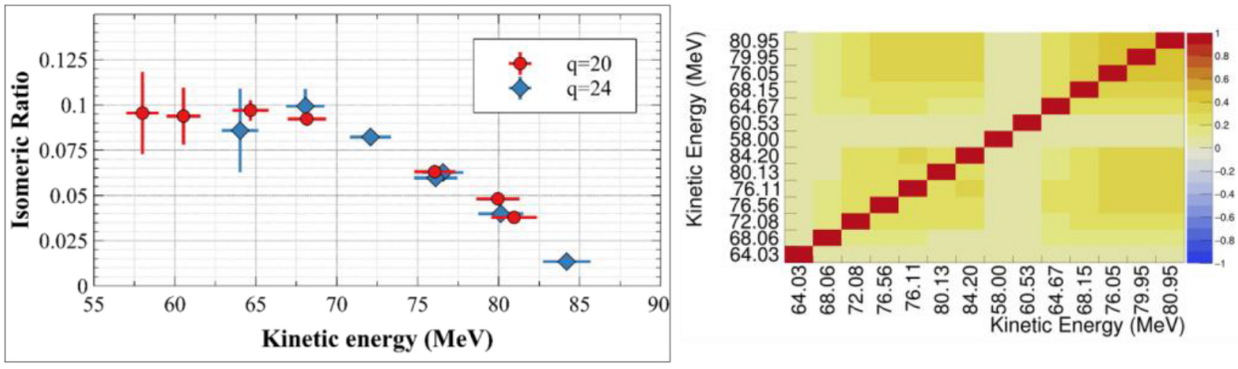

Figure 6. Isomeric Ratio of ^{132}Sn from thermal neutron induced fission of ^{241}Pu measured at two different ionic charge selections (left) and the associated covariance matrix (right). The kinetic energies are corrected from the relative evolution of the energy loss during the experimental campaign.

Once the input parameters, A, Z, E^* and J^{π} are provided, a cascade can start. The above-mentioned models and experimental level schemes are used to calculate the isomeric ratio for a particular E^* and J^{π} combination. The E^* has a range starting at the energy of the isomeric state up to the neutron separation energy. For each excitation energy, a range J^{π} of values ($0^{\pm}$ to $30^{\pm}$) is given. For each of these J^{π} values, an IR ($IR_{FIF}(E^*, J^{\pi})$) is calculated by FIFRELIN. To compare these results with the experimental data, the results are averaged by the equation given below:

$$IR_{FIF}(E^*, J_{rms}) = \sum_{J} \sum_{\pi} P(\pi) P(J) IR_{FIF}(E^*, J^{\pi}) \tag{2}$$

$$\text{where } P(J) \propto (2J+1) \exp\left(-\frac{\left(J+\frac{1}{2}\right)^2}{J_{rms}^2}\right) \tag{3}$$

$$\text{and } P(\pi) = P(\pm 1) = \frac{1}{2} \tag{4}$$

The Likelihood method is used to adjust the spin cut-off (J_{rms},) which in that case is a free parameter

$$L(E^*, J_{rms} \mid E_k) \propto \exp\left(-\frac{\left(IR_{exp}(E_k) - IR_{FIF}(E^*, J_{rms})\right)^2}{2\left(\sigma_{exp}^2, \sigma_{FIF}^2\right)}\right) \tag{5}$$

where, $IR_{exp}(E_k)$ and σ_{exp} are the isomeric ratios and their uncertainty obtained from the experiments that is dependent on the selected kinetic energy from LOHENGRIN. σ_{FIF} is the uncertainty obtained from FIFRELIN.

5 Results and conclusion

Combining the FIFRELIN calculations with the experimental results, we were able to extract the J_{rms} value as a function of kinetic energy. Figure 7 depicts the results from this work, which have been compared to the results obtained by using a ^{235}U target [5]. It can be seen that the J_{rms} value obtained from two different fissioning systems are quite similar. Also for this work, one can observe a flat plateau-like region at lower kinetic energies. Further experiments and calculations need to be carried out to explain this phenomenon. Experimental results from this work have been further compared with the calculations using the Madland-England (M.E.) model and the GEF code. This can be seen in Table 1. The M.E. model uses the assumption that the isomeric ratio is only dependant on the spin of both the ground state and the isomeric state. Furthermore, it works on the supposition that all the fission fragments are characterised by a spin cut-off value of (7.5±0.5) h, which gives an isomeric ratio of 0.642±0.039 for ^{132}Sn (M.E. (a)). By using the isomeric ratio from this work, which is 0.0719±0.0016, a J_{rms} of 2.8±0.1 (M.E. (b)) is obtained from the M.E. model. We clearly observe a mismatch between the experimental results and those obtained from the M.E. model for ^{132}Sn.

Table 1. Comparison of results: In M.E. (a), $\overline{\mathbf{J}_{rms}}$ is set to 7.5 h and the IR is calculated by using M.E. model. In M.E. (b), the IR is set equivalent to our experimental result and the $\overline{\mathbf{J}_{rms}}$ is calculated using the same model.

Experiments	$\overline{IR}$	$\overline{J_{rms}}$ ($\hbar$)
This work (^{241}Pu)	0.0719±0.0016	4.8±0.1
^{235}U [5]	0.054±0.006	4.7±0.2
Models		
Madland-England (a)	0.642±0.039	7.5±0.5
Madland-England (b)	0.0719±0.0016	2.8±0.1
GEF [22]	0.234	6.65±0.03

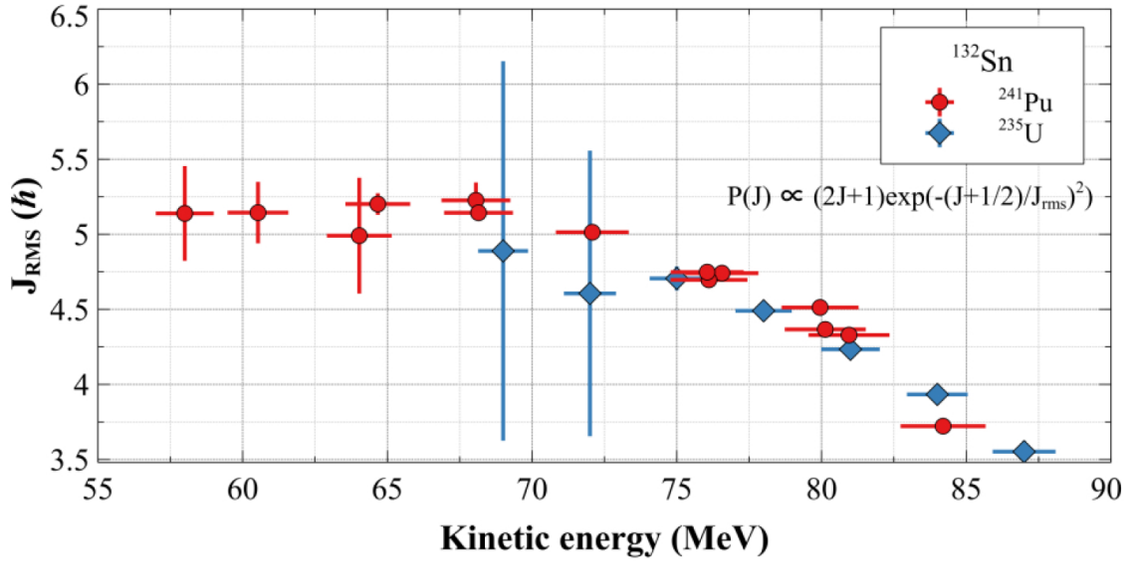

Figure 7. Spin of ^{132}Sn and its dependence on kinetic energy using ^{241}Pu and ^{235}U targets. The kinetic energies are corrected from the relative evolution of the energy loss during the experimental campaign.

In conclusion, the dependence of the isomeric ratios of the fission products on their kinetic energy was obtained. Using statistical analysis, along with FIFRELIN calculations involving level density models, gamma strength functions, spin cut-off models and internal conversion coefficients, we were able to determine the J_{rms} value for each of the isomeric ratios obtained. Furthermore, it can be observed that the J_{rms} values for two different fissioning systems are quite similar and follow a similar trend. For nuclei such as ^{132}Sn, the results from the experiments should be taken into account for the nuclear data evaluations instead of using codes or models to compute them. In this same experimental campaign, experiments were carried out on other isotopes of Sn as well. It would be very interesting to see how the J_{rms} value changes with change in mass for the same element.

The authors would like to thank and express our gratitude towards the support staff of the ILL as well as the staff involved from CEA-Cadarache and LPSC Grenoble. This work has been supported by the NEEDS project, by CNRS and by CEA. This work has been done in collaboration with CEA-Cadarache, LPSC Grenoble and ILL.

Raw data of this experiment are available via ref. [23].

References

[1] O. Hahn, F.W. Strassmann, Naturwissenschaften **27**, 11 (1939)
[2] L. Meitner, O.R. Frisch, Nature **142**, 239 (1939)
[3] D. Madland, T. England, Nuclear science and Engineering **64**, 859-865 (1977)
[4] D. Tarrío, L.S. Leong, L. Audouin, I. Duran, C. Paradela, et al., Nuclear Instruments and Methods in Physics Research A **743**, 79-85 (2014)
[5] A. Chebboubi, G. Kessedjian, O. Litaize, O. Serot, H. Faust, D. Bernard, A. Blanc, U. Köster, O. Méplan, P. Mutti, C. Sage, Physics Letters B **775**, 190-195 (2017)
[6] A. Al-Adili, V. Rakopoulos, A. Solders, European Physical Journal A **55**, 61 (2019)
[7] V. Rakopoulos, M. Lantz, S. Pomp, A. Solders, A. Al-Adili, L. Canete, T. Eronen, A. Jokinen, A. Kamkainen, A. Mattera, I.D. Moore, D.A. Nesterenko, M. Reponen, S. Rinta-Antila, A. de Roubin, M. Vilén, M. Österlund, H. Penttilä, Physical Review C **99**, 014617 (2019)
[8] P. Armbruster, M. Asghar, J.P. Bocquet, R. Decker, H. Ewald, J. Greif, E. Moll, B. Pfeiffer, H. Schrader, F. Schussler, G. Siegert, H. Wollnik, Nuclear instruments and Methods **139**, 213-222 (1976)
[9] "About ILL; What is The ILL" Institut Laue-Langevin, [Online]. Available: https://www.ill.eu/about-ill/what-is-the-ill/
[10] "PN1 Fission-product spectrometer; PN1 characteristics" [Online]. Available: https://www.ill.eu/users/instruments/instruments-list/pn1/characteristics/
[11] G. Fioni, H.R. Faust, M. Gross, M. Hesse, P. Armbruster, F. Gönnenwein, Nuclear Instruments and Methods in Physics Research A **332**, 175-180 (1993)
[12] Y. Khazov, A.A. Rodionov, S. Sakharov, B. Singh, Nuclear Data Sheets **104**, 497-790 (2005)
[13] A. Fitzler, *Program TV,* Cologne: Institute for Nuclear Physics
[14] A. Chebboubi, *Contribution à l'étude de la fission nucléaire : de LOHENGRIN à FIPPS*, PhD thesis from Université de Grenoble (2015)
[15] S. Julien-Laferrière, A. Chebboubi, G. Kessedjian, O. Serot, EPJ Nuclear Sci. Technol., **4**, 25 (2018)
[16] O. Litaize, O. Serot, L. Berge, The European Physical Journal A **51**, 177 (2015)

[17] R. Capote, M. Herman, P. Oblozinsky, P.G. Young, S. Goriely, T. Belgya, A.V. Ignatyuk, A.J. Koning, S. Hilaire, V.A. Plujko, M. Avrigeanu, O. Bersillon, M. B. Chadwick, T. Fukahori, Z. Ge, Y. Han, S. Kailas, J. Kopecky, V.M. Maslov, G. Reffo, M. Sin, E. Sh. Soukhovitskii, P. Talou, Nuclear Data Sheets **110**, 3107-3214 (2009)

[18] M. Verpelli and R. Capote, "Structure of RIPL discrete level library files," [Online]. Available: https://www-nds.iaea.org/RIPL-3/levels/levels-readme.html

[19] J. Kopecky, M. Uhl, Physical Review C **41** (1990)

[20] T. Kibédi, T.W. Burrows, M.B. Trzhaskovskaya, P.M. Davidson and C.W. Nestor Jr, Nuclear Instruments and Methods in Physics Research A **589**, 202-229 (2008)

[21] A.J. Koning, J.P. Delaroche, Nuclear Physics A **713**, 321-310 (2003)

[22] K.H. Schmidt, B. Jurado, C. Amouroux and C. Schmitt, Nuclear Data Sheets **131**, 107-221 (2016)

[23] G. Kessedjian, D. Bernard, A. Blanc, A. Chebboubi, H. Faust, Y.H. Kim, U. Köster, O. Litaize, O. Méplan, J.N. Nicholson, M. Ramdhane, C. Sage and O. Serot, ILL, doi:10.5291/ILL-DATA.3-01-640 (2018)